

ynogkm: A New Public Code For Calculating time-like Geodesics In The Kerr-Newmann Spacetime

Xiao-Lin. Yang^{1,2,3} and Jian-Cheng. Wang^{2,3}

¹ Yunnan Astronomical Observatory, Chinese Academy of Sciences, Kunming 650011, P.R. China

² Key Laboratory for the Structure and Evolution of Celestial Objects, Chinese Academy of Sciences, Kunming 650011, P.R. China

³ University of Chinese Academy of Sciences, Beijing 100049, P.R. China

Preprint online version: May 19, 2018

ABSTRACT

In this paper we present a new public code, named *ynogkm*, for the fast calculation of time-like geodesics in the Kerr-Newmann (K-N) spacetime, which is a direct extension of *ynogk* calculating null geodesics in a Kerr spacetime. Following the strategies used in *ynogk*, we also solve the equations of motion analytically and semi-analytically by using Weierstrass' and Jacobi's elliptic functions and integrals, in which the Boyer-Lidquist (B-L) coordinates r , θ , ϕ , t and the proper time σ are expressed as functions of an independent variable p (Mino time). All of the elliptic integrals are computed by Carlson's elliptic integral method, which guarantees the fast speed of the code. Finally the code is applied to a couple of toy problems.

Key words. accretion, accretion disks - black hole physics - relativistic processes - methods: numerical

1. Introduction

In the vicinity of the black hole and any other compact objects, the gravitational field is extremely strong and the spacetime is significant warped and twisted. Thus the general relativity effects can not be ignored. The motion of free photons and test particles in this curved spacetime is along geodesics if we do not consider the external forces or perturbations exerting on them. The assumption that photons and particles propagate along geodesic trajectories is valid in most astrophysics contexts. The fast calculation of the null and time-like geodesics in curved spacetime is significantly important and has been widely used in the Astrophysical researches (e.g., Cunningham & Bardeen (1973); Luminet (1979); Rauch & Blandford (1994); Hackmann (2010)).

The calculation and applications of null geodesics in a curved spacetime, especially in a Kerr spacetime, have been discussed by many authors in different attempts to date (Dexter & Agol (2009); Hackmann (2010); Hackmann & Xu (2013); Chan et al. (2013); Yang & Wang (2013), and the references therein). To compute the geodesics one can integrate a set of second-order differential equations in any relativistic spacetime directly, or evaluate a set of elliptic integrals of motion in a K-N spacetime. In the present paper we focus on the latter approach. There are four constants for any geodesic motions in a K-N spacetime (Carter 1968), which makes the reduction of the order of motion equations possible.

To get the optical appearance of a star orbiting around an extreme Kerr black hole, Cunningham & Bardeen (1973) calculated the null geodesics in a Kerr spacetime based on the elliptic integral method and proposed the impact parameters for the first time. After that a method called ray-tracing was developed (e.g., Luminet (1979)). Rauch & Blandford (1994) researched the optical caustics in a Kerr spacetime with an attempt to explain rapid X-ray variability in AGN. As a gift they presented, in tabular form, cases need to be considered for the calculation of both the null and time-like geodesics in a Kerr spacetime.

Similar discussions and results are also given by Li et al. (2005) in their Appendix.

The cases discussed by the above authors are very detailed but also very complicated. As discussed in Yang & Wang (2013), this sophisticated situation can be significantly simplified by the introductions of the Mino time p (Mino 2003) and the Weierstrass' elliptic integrals and functions (also see Hackmann (2010); Hackmann & Xu (2013), in which how to solve the equations of geodesic motion in a more general instead of restricting to the Kerr or K-N spacetime are discussed systematically by Mino time and all kinds of elliptic functions). The Carlson's elliptic approach is quite suitable and efficient for evaluating elliptic integrals and functions, which has been demonstrated by Dexter & Agol (2009) and Yang & Wang (2013).

Motivated by the above discussions and the fact that there is no a public code available in the present time to calculate time-like geodesics in a K-N spacetimes for all coordinates (including the proper times) at the same time, we extend the scheme of Yang & Wang (2013) from null geodesics in a Kerr spacetime to time-like geodesics in a K-N spacetime in this paper. As a result a new public code, named *ynogkm* (Yun-Nan Observatory Geodesic in a Kerr-Newmann spacetime for Massive particles) is developed.

Analogous to *ynogk*, in *ynogkm* we also express the B-L coordinates r , θ , ϕ , t and the proper time σ as functions of the Mino time p semianalytically by using Weierstrass' and Jacobi's elliptic functions and integrals. Such treatment makes the practical applications to be handled conveniently. The Mino time p is an integral value along a particular geodesic. All of the elliptical integrals are computed by Carlson's approach. With a similar way to *ynogk*, we also discuss how to compute the constants of motion from the initial conditions, i.e., the initial four-momentum of the particles measured under the local nonrotating frame (LNRF, Bardeen et al. (1972)). For a massive particle with electric charge in a K-N spacetime, the number of constants of motion becomes 4. For a photon whose rest mass μ_m and electric charge ϵ are both zero, the number of constants of motion

is 2. When taking μ_m and ϵ to be zero, the discussions here are reduced to those for null geodesics.

The paper is organized as follows. In section 2 we give the equations of motion for an electric charged massive particle in a K-N spacetime. In section 3 we discuss the expressions of the B-L coordinates and proper time as functions of parameter p . Then we reduce all of the elliptic integrals to standard forms which are evaluated by Carlson's approach. Next we discuss the calculation of constants of motion from initial conditions in section 4. A brief introduction and discussion about the code are given in section 5. In section 6 we demonstrate the applications of our code to toy problems in the literature. Finally a brief summary is presented in section 7. Throughout this paper the natural unit is used, in which the constants $G=c=1$. The mass of central black hole M is also taken to be 1, unless otherwise stated.

2. The equations of motion for time-like geodesics

We assume that the spin and electric charge of the black hole are a and e respectively. Using the notation of Bardeen et al. (1972), we can write the Kerr-Newman metric under the B-L coordinate as

$$ds^2 = -e^{2\nu} dt^2 + e^{2\psi} (d\phi - \omega dt)^2 + e^{2\mu_1} dr^2 + e^{2\mu_2} d\theta^2, \quad (1)$$

where

$$e^{2\nu} = \frac{\Sigma \Delta}{A}, \quad e^{2\psi} = \frac{\sin^2 \theta A}{\Sigma}, \quad e^{2\mu_1} = \frac{\Sigma}{\Delta}, \quad (2)$$

$$e^{2\mu_2} = \Sigma, \quad \omega = \frac{(2r - e^2)a}{A},$$

and

$$\Delta = r^2 - 2r + a^2 + e^2, \quad \Sigma = r^2 + a^2 \cos^2 \theta, \quad (3)$$

$$A = (r^2 + a^2)^2 - \Delta a^2 \sin^2 \theta.$$

Carter (1968) gave the first-order differential equations of motion for electric charged massive particles as follows:

$$\Sigma \frac{dr}{d\lambda} = \pm \sqrt{R_r}, \quad (4)$$

$$\Sigma \frac{d\theta}{d\lambda} = \pm \sqrt{\Theta_\theta}, \quad (5)$$

$$\Sigma \frac{d\phi}{d\lambda} = -(aE - \frac{L}{\sin^2 \theta}) + \frac{aT}{\Delta}, \quad (6)$$

$$\Sigma \frac{dt}{d\lambda} = -a(aE \sin^2 \theta - L) + \frac{(r^2 + a^2)T}{\Delta}, \quad (7)$$

where

$$T = E(r^2 + a^2) - La + e\epsilon r, \quad (8)$$

$$R_r = T^2 - \Delta[\mu_m^2 r^2 + (L - aE)^2 + Q], \quad (9)$$

$$\Theta_\theta = Q - \cos^2 \theta [a^2(\mu_m^2 - E^2) + L^2 / \sin^2 \theta], \quad (10)$$

and $\lambda = \tau/\mu_m$, τ is the proper time, μ_m is the rest mass of the particle, Q is the Carter constant, E is the energy tested by an observer at infinity, L is the angular momentum of the particle about the black hole spin axis, and ϵ is the electric charge of the particle. From Equations (4)-(7) we can obtain the expression of the four-momentum for a particle

$$p_\mu = g_{\mu\nu} \frac{dx^\nu}{d\lambda} = (-E, \pm \frac{\sqrt{R_r}}{\Delta}, \pm \sqrt{\Theta_\theta}, L). \quad (11)$$

Equivalently the equations of motion with integral forms can be written as:

$$\pm \int^\theta \frac{d\theta}{\sqrt{\Theta_\theta}} = \pm \int^r \frac{dr}{\sqrt{R_r}}, \quad (12)$$

$$\sigma = \frac{\tau E}{\mu_m} = \int^\theta \frac{Ea^2 \cos^2 \theta}{\sqrt{\Theta_\theta}} d\theta + \int^r \frac{Er^2}{\sqrt{R_r}} dr, \quad (13)$$

$$t = \sigma + 2 \int^r \frac{N_r}{\Delta \sqrt{R_r}} dr, \quad (14)$$

$$\phi = \int^\theta \frac{L \csc^2 \theta}{\sqrt{\Theta_\theta}} d\theta + a \int^r \frac{r(2E - e\epsilon) - (Ee^2 + La)}{\Delta \sqrt{R_r}} dr, \quad (15)$$

where

$$N_r = (2E + e\epsilon)r^3 - Ee^2 r^2 + [2a(Ea - L) + a^2 e\epsilon]r - e^2 a(Ea - L). \quad (16)$$

Here σ is a new variable, which is related to the proper time τ of the particle. For a photon, it becomes an affine parameter.

In many cases we only need the equations of motion with integral forms. But in two special cases, i.e., the equatorial plane motion and the spherical motion, we need the differential equations of motion. In the former case, the particle is confined in the equatorial plane, one has $Q = 0$, $\theta \equiv \pi/2$, and thus $\Theta_\theta \equiv 0$. Then the equations of motion with integral forms become invalid, since $\Theta_\theta \equiv 0$ appears in the denominator. But from the differential equations we can get the right equations to describe the plane motion. From Equation (4), we have

$$\sigma = \lambda E = \int^r \frac{Er^2}{\sqrt{R_r}} dr. \quad (17)$$

Dividing both sides of Equation (4) by Equation (7), we get

$$t = \sigma + \int^r \frac{N_r}{\Delta \sqrt{R_r}} dr. \quad (18)$$

Similarly, from Equations (4) and (6) we get

$$\phi = L \int^r \frac{dr}{\sqrt{R_r}} + a \int^r \frac{r(2E - e\epsilon) - (Ee^2 + La)}{\Delta \sqrt{R_r}} dr. \quad (19)$$

For spherical motion, we have $R_r \equiv 0$, thus the equations of motion with integral forms become invalid, because R_r appears in the denominator. Similarly, from Equation (5) we obtain

$$\sigma = E \int d\lambda = Ea^2 \int^\theta \frac{\cos^2 \theta}{\sqrt{\Theta_\theta}} d\theta + Er^2 \int^\theta \frac{d\theta}{\sqrt{\Theta_\theta}}. \quad (20)$$

From Equations (5) and (7) we get

$$t = \sigma + \frac{N_r}{\Delta} \int^\theta \frac{d\theta}{\sqrt{\Theta_\theta}}. \quad (21)$$

And from Equations (5) and (6) we get

$$\phi = L \int^\theta \frac{\csc^2 \theta}{\sqrt{\Theta_\theta}} d\theta + a \frac{r(2E - e\epsilon) - (Ee^2 + La)}{\Delta} \int^\theta \frac{d\theta}{\sqrt{\Theta_\theta}}. \quad (22)$$

With Equations (12)-(22), we can calculate the geodesics by evaluating the elliptical integrals, instead of solving the differential equations of motion, and can also express the B-L coordinates and proper time as functions of a parameter p . In the next section we discuss how to get these functions semianalytically by elliptical functions and integrals.

3. The expressions of B-L coordinates and proper time as functions of p

3.1. The turning points

As discussed in Yang & Wang (2013), when we introduce a new parameter p with following definition from Equation (12)

$$p = \pm \int^r \frac{dr}{\sqrt{R}} = \pm \int^\mu \frac{d\mu}{\sqrt{\Theta_\mu}}, \quad (23)$$

we can get functions $r(p)$, $\mu(p)$, $\phi(p)$, $t(p)$, and $\sigma(p)$ by the equations of motion with integral forms, where $\mu = \cos \theta$ and

$$R(r) = \frac{R_r}{E^2} = (1 - m^2)r^4 + 2(m^2 + e\varepsilon)r^3 - [q + \lambda^2 + a^2(m^2 - 1) + e^2(m^2 - \varepsilon^2)]r^2 + 2[q + (a - \lambda)^2 + ea\varepsilon(a - \lambda)]r - e^2(a - \lambda)^2 - (a^2 + e^2)q, \quad (24)$$

$$\Theta_\mu(\mu) = \frac{\Theta_\theta \sin^2 \theta}{E^2} = a^2(m^2 - 1)\mu^4 - [q + \lambda^2 + a^2(m^2 - 1)]\mu^2 + q. \quad (25)$$

Since the signs before the integrals are the same with dr and $d\theta$, the parameter p monotonously increases along a particular geodesic. Here $\lambda = L/E$, $q = Q/E^2$, $m = \mu_m/E$, and $\varepsilon = \epsilon/E$, which are defined as constants of motion throughout this paper. Because R and Θ_μ are quartic (when $m \neq 1$) or cubic (when $m = 1$) polynomials, the integrals about r and μ are elliptical integrals, which are reduced to the Weierstrass' standard elliptic integrals (or Legendre's ones when equation $R(r) = 0$ has no real roots).

Since both R and Θ_θ appear under the radical sign in the equations of motion, they must be nonnegative. The critical points satisfying $R(r) = 0$ or $\Theta_\theta(\theta) = 0$ are so-called turning points, in which the corresponding coordinate velocity is zero. When the motion of a particle is bounded in r or in θ coordinate, two turning points exist for the coordinate. We use r_{tp_1} , r_{tp_2} , and θ_{tp_1} , θ_{tp_2} to denote the coordinates of these points, and assume that $r_{tp_1} \leq r_{tp_2}$, $\theta_{tp_1} \leq \theta_{tp_2}$. Since $p_r = \pm \sqrt{R_r}/\Delta$, $p_\theta = \pm \sqrt{\Theta_\theta}$, when $p_r = 0$ or $p_\theta = 0$ at the initial point, we have $R_r(r_{ini}) = 0$, $\Theta_\theta(\theta_{ini}) = 0$, implying that the initial point is a turning point and r_{ini} (or θ_{ini}) is equal to one of r_{tp_1} , r_{tp_2} (or θ_{tp_1} , θ_{tp_2}). Then we have $r_{ini} \in [r_{tp_1}, r_{tp_2}]$ and $\theta_{ini} \in [\theta_{tp_1}, \theta_{tp_2}]$.

When r_{tp_2} does not exist at all (or equivalently, $r_{tp_2} = \infty$) and $r_{tp_1} > r_h$, the particle will eventually go to infinity far away. When r_{tp_1} does not exist (or $r_{tp_1} < r_h$) and $r_{tp_2} > r_h$, then the particle will eventually fall into the event horizon of the black hole. If (1) both r_{tp_1} and r_{tp_2} do not exist, this case equivalently corresponds to that the equation $R(r) = 0$ has no real roots; or (2) r_{tp_2} does not exist and r_{tp_1} exists but $r_{tp_1} < r_h$, for the both cases the particle can move from infinity to the event horizon freely.

To get the θ coordinate of a turning point, we usually solve the equation $\Theta_\mu(\mu) = 0$ to get μ_{tp} ($= \cos \theta_{tp}$) instead of solving the equation $\Theta_\theta(\theta) = 0$. The roots of two equations are exactly the same except these special cases with constant $\lambda = 0$. The equation $\Theta_\mu(\mu) = 0$ with $\lambda = 0$ has real roots ± 1 , or $0, \pi$, which are not the roots of equation $\Theta_\theta(\theta) = 0$, indicating that a particle with $\lambda = 0$ can move from 0 to π freely and can go through the spin axis due to non-zero poloidal velocity $p_\theta = \pm \sqrt{\Theta_\theta}$ at the spin axis. Meanwhile, the particle changes the sign of its angular velocity $d\theta/d\lambda$, and its azimuthal coordinate jumps from ϕ to $\phi \pm \pi$ (Shakura 1987) instantaneously.

Table 1. Expression of $\mu(p)$

Case	$\mu(p)$
$a \neq 0$	$\mu(p) = \frac{b_0}{4\wp(p + \Pi_\mu; g_2, g_3) - b_1} + \mu_{tp_1}, \quad (26)$
$m \neq 1$	$b_0 = 4a^2(m^2 - 1)\mu_{tp_1}^3 - 2[q + \lambda^2 + a^2(m^2 - 1)]\mu_{tp_1},$ $b_1 = 2a^2(m^2 - 1)\mu_{tp_1}^2 - \frac{1}{3}[q + \lambda^2 + a^2(m^2 - 1)],$ $b_2 = \frac{4}{3}a^2(m^2 - 1)\mu_{tp_1}, \quad b_3 = a^2(m^2 - 1), \quad g_2, g_3!$
Case	Π_μ
$a \neq 0$	$ \Pi_\mu = \wp^{-1}[z(\mu_{ini}); g_2, g_3] , \quad z(\mu) = \frac{b_0}{4} \frac{1}{(\mu - \mu_{tp_1})} + \frac{b_1}{4},$
$m \neq 1$	$\Pi_\mu \begin{cases} > 0, & p_\theta > 0, \\ = \pm n\omega', & \theta_{ini} = \theta_{tp_1} \\ = \pm(\frac{1}{2} + n)\omega', & \theta_{ini} = \theta_{tp_2} \\ < 0, & p_\theta < 0. \end{cases}$

$$^1 g_2 = \frac{3}{4}(b_1^2 - b_0b_2), g_3 = \frac{1}{16}(3b_0b_1b_2 - 2b_1^3 - b_0^2b_3).$$

$$^2 \text{ where } \omega' \text{ is the real period of } \wp(z; g_2, g_3) \text{ and } n = 0, 1, 2, \dots$$

Table 2. Expression of $r(p)$

Case	$r(p)$
1	$r(p) = \frac{b_0}{4\wp(p + \Pi_r; g_2, g_3) - b_1} + r_{tp_1}, \quad (27)$
2	$r_\pm(p) = v + \frac{-(u - v) \pm s(\lambda_1 - \lambda_2)z(p) \sqrt{1 - z(p)^2}}{(\lambda_1 - \lambda_2)z(p)^2 - (\lambda_1 - 1)},$ $z(p) = \text{sn}(s \sqrt{\lambda_1(1 - m^2)} p \mp \Pi_r k^2),$ $r(p) = \begin{cases} r_-(p), & p_r > 0, \\ r_+(p), & p_r < 0. \end{cases} \quad (28)$
3	$r_\pm(p) = u + \frac{-\lambda_1(u - v)/(\lambda_1 + 1) \pm wz(p) \sqrt{1 - z(p)^2} [(1 + \lambda_1)/k^2]^2}{1 - z(p)^2 [(1 + \lambda_1)/k^2]},$ $z(p) = \text{sn}(s \sqrt{\lambda_2(1 - m^2)} p \mp \Pi_r k^2),$ $r(p) = \begin{cases} r_-(p), & p_r > 0, \\ r_+(p), & p_r < 0. \end{cases} \quad (29)$
4	$r(p) = \frac{1}{b_0} [4\wp(p + \Pi_r; g_2, g_3) - b_1], \quad (30)$
5	$r(p) = \frac{1}{b_0} \left[4e_2 - b_1 - \frac{4(e_1 - e_2)(e_2 - e_3)}{\wp(p + \Pi_\xi; g_2, g_3) - e_2} \right]. \quad (31)$

3.2. μ and r coordinates

In this section we express μ and r as functions of parameter p , i.e., $\mu = \mu(p)$, $r = r(p)$. The procedure to get these explicit expressions for electric charged massive particles is quite tedious but similar to the procedure for photons (one can refer to the discussions in Yang & Wang (2013)). Thus there is no need to present the details of the procedure. For the purpose of easier referring we present expressions of $\mu(p)$, $r(p)$ in tabular form. See table 3.2.

For r , there are five cases:

1. $m \neq 1$ and equation $R(r) = 0$ has one real root at least.
2. $1 - m^2 > 0$ (or $|E| > \mu_m$) and $R(r) = 0$ has no real roots.
3. $1 - m^2 < 0$ (or $|E| < \mu_m$) and $R(r) = 0$ has no real roots.
4. $|m| = 1$ (or $|E| = \mu_m$) and the geodesic is unbounded.
5. $|m| = 1$ (or $|E| = \mu_m$) and the geodesic is bounded.

In case 1, $R(r) = 0$ with $m \neq 1$ at least has one real root. We do not care how many real roots the equation has and their practical distribution. When the equation $R(r) = 0$ has real roots,

Table 3. Definitions of Table 2.

Case	$b_0, b_1, b_2, b_3, g_2, g_3, \lambda_1, \lambda_2, k^2$	Π_r, Π_ξ
1	$b_0 = 4(1 - m^2)r_{\text{tp}_1}^3 + 6(m^2 + e\varepsilon)r_{\text{tp}_1}^2 - 2[q + \lambda^2 + a^2(m^2 - 1) + e^2(m^2 - \varepsilon^2)]r_{\text{tp}_1} + 2[q + (\lambda - a)^2 + ae\varepsilon(a - \lambda)],$ $b_1 = 2(1 - m^2)r_{\text{tp}_1}^2 + 2(m^2 + e\varepsilon)r_{\text{tp}_1} - \frac{1}{3}[q + \lambda^2 + a^2(m^2 - 1) + e^2(m^2 - \varepsilon^2)]r_{\text{tp}_1},$ $b_2 = \frac{4}{3}(1 - m^2)r_{\text{tp}_1} + \frac{2}{3}(m^2 + e\varepsilon), \quad b_3 = 1 - m^2, \quad g_2, \quad g_3^1$	$ \Pi_r = \wp^{-1}[z(r_{\text{ini}}); g_2, g_3] , \quad z(r) = \frac{b_0}{4} \frac{1}{(r - r_{\text{tp}_1})} + \frac{b_1}{4},$ $\Pi_r = \begin{cases} \Pi_r , & p_r > 0, \\ \pm n\omega'; & r_{\text{ini}} = r_{\text{tp}_1} \\ \pm(\frac{1}{2} + n)\omega', & r_{\text{ini}} = r_{\text{tp}_2} \\ - \Pi_r , & p_r < 0, \end{cases}$
2	$\lambda_{1,2} = \frac{(u - v)^2 + w^2 + s^2 \pm \sqrt{[w^2 + s^2 + (u - v)^2]^2 - 4s^2w^2}}{2s^2}, \quad (32)$ $\lambda_1 > 1 > \lambda_2 > 0, \quad k^2 = \frac{\lambda_1 - \lambda_2}{\lambda_1},$	$\Pi_r = \text{sn}^{-1}[z(r_{\text{ini}}) k^2] , \quad \alpha_1 = \frac{\lambda_1 v - u}{\lambda_1 - 1},$ $z(r) = \sqrt{\frac{\lambda_1 - 1}{\lambda_1 - \lambda_2}} \frac{(r - \alpha_1)}{\sqrt{(r - v)^2 + s^2}}, \quad (33)$
3	$\lambda_{1,2} = \frac{-(u - v)^2 - w^2 - s^2 \pm \sqrt{[w^2 + s^2 + (u - v)^2]^2 - 4s^2w^2}}{2s^2}, \quad (34)$ $0 > \lambda_1 > -1 > \lambda_2, \quad k^2 = \frac{\lambda_2 - \lambda_1}{\lambda_2},$	$\Pi_r = \text{sn}^{-1}[z(r_{\text{ini}}) k^2] , \quad \alpha_1 = \frac{\lambda_1 v + u}{\lambda_1 + 1},$ $z(r) = \sqrt{\frac{\lambda_1 - \lambda_2}{-\lambda_2(\lambda_1 + 1)}} \frac{(r - \alpha_1)}{\sqrt{(r - u)^2 + w^2}}, \quad (35)$
4	$b_0 = 2(1 + e\varepsilon), \quad b_1 = -\frac{1}{3}[q + \lambda^2 + e^2(1 - \varepsilon^2)],$ $b_2 = \frac{2}{3}[q + (a - \lambda)^2 + ea\varepsilon(a - \lambda)], \quad b_3 = -e^2(a - \lambda)^2 - (a^2 + e^2)q,$ $g_2, \quad g_3^1$	$ \Pi_r = \wp^{-1}[z(r_{\text{ini}}); g_2, g_3] , \quad z(r) = \frac{b_0}{4}r + \frac{b_1}{4},$ $\Pi_r = \begin{cases} -\text{sign}(b_0) \Pi_r , & p_r > 0, \\ \pm(\frac{1}{2} + n)\omega', & r_{\text{ini}} = r_{\text{tp}_1} \\ \text{sign}(b_0) \Pi_r , & p_r < 0, \end{cases}$
5	$b_0 = 2(1 + e\varepsilon), \quad b_1 = -\frac{1}{3}[q + \lambda^2 + e^2(1 - \varepsilon^2)],$ $b_2 = \frac{2}{3}[q + (a - \lambda)^2 + ea\varepsilon(a - \lambda)], \quad b_3 = -e^2(a - \lambda)^2 - (a^2 + e^2)q,$ $g_2, \quad g_3^1$ $e_1, e_2, e_3 \text{ are three real roots of } 4z^3 - g_2z - g_3 = 0 \text{ and } e_3 < e_2 < e_1.$	$ \Pi_\xi = \wp^{-1}[\xi(r_{\text{ini}}); g_2, g_3] ,$ $\xi(r) = e_2 - \frac{(e_1 - e_2)(e_2 - e_3)}{z(r) - e_2}, \quad z(r) = \frac{b_0}{4}r + \frac{b_1}{4},$ $\Pi_\xi = \begin{cases} -\text{sign}(b_0) \Pi_\xi , & p_r > 0, \\ \pm(\frac{1}{2} + n)\omega', & z(r_{\text{ini}}) = e_3, \\ \pm n\omega', & z(r_{\text{ini}}) = e_2, \\ \text{sign}(b_0) \Pi_\xi , & p_r < 0. \end{cases}$

¹ See the footnote of Table 1.

Table 4. Expression of p

Case	p
1, 4, 5	$p = \int^z \frac{dz}{\sqrt{4z^3 - g_2z - g_3}}, \quad (36)$
2	$p = \int^z \frac{dz}{s\sqrt{\lambda_1(1 - m^2)}\sqrt{(1 - z^2)(1 - k^2z^2)}}, \quad (37)$
3	$p = \int^z \frac{dz}{s\sqrt{\lambda_2(1 - m^2)}\sqrt{(1 - z^2)(1 - k^2z^2)}}. \quad (38)$

r_{tp_1} (or r_{tp_2}) does exist, and can be easily determined with given r_{ini}^1 .

In cases 2 and 3, $R(r) = 0$ has no real roots, but two pairs of complex conjugate roots written as:

$$r_1 = u + iv, \quad r_2 = u - iv, \quad (39)$$

$$r_3 = w + is, \quad r_4 = w - is. \quad (40)$$

To avoid dealing with complex integral we use Jacobi's elliptic function to express r instead of Weierstrass' ones.

For cases 4 and 5, $1 - m^2 = 0$, thus $R(r)$ reduces to

$$R(r) = 2(1 + e\varepsilon)r^3 - [q + \lambda^2 + e^2(1 - \varepsilon^2)]r^2 + 2[q + (a - \lambda)^2 + ea\varepsilon(a - \lambda)]r - e^2(a - \lambda)^2 - (a^2 + e^2)q, \quad (41)$$

From the expression of $r(p)$ in Equation (30), we know that when $p \pm \Pi_r = \omega'$, $\wp(p \pm \Pi_r; g_2, g_3) = \infty$, i.e., $r(p) = \infty$, meaning that no matter what initial value p_r takes, the particle shall go to infinity eventually. As a result, the particular geodesic is unbounded.

¹ Actually r_{tp_1} exists for all cases that we discussed in this paper.

3.3. ϕ, t coordinates and the proper time σ

As discussed in Yang & Wang (2013), the expressions of ϕ, t , and σ as functions of parameter p can be converted to evaluate the elliptic integrals appeared in the equations of motion with a given p . We divide the process into two steps. In the first step, the path and limits of the integrals are determined. In the second step, the integrals are reduced to standard forms, which are evaluated by Carlson's approach.

3.3.1. The path and limits of integrals

For convenience, we use F_r and F_μ to represent the complicated integrands in integrals of r and μ respectively.

The path is not monotonic when one or more than one turning points exist for r and μ . The path is divided into several parts, in which each one has the maximum monotonic length, and the integrals are the sum of all individual part. In Figure 1, the integral path of r coordinate for a particular bounded geodesic is illustrated schematically. The motion of the particle is confined between two turning points, r_{tp_1} and r_{tp_2} .

There are four important points in a particular path for r (or for μ), they are related to the integral limits. They are: 1. the initial position r_{ini} (or μ_{ini}); 2. the two turning points, r_{tp_1} and r_{tp_2} (or $\mu_{\text{tp}_1}, \mu_{\text{tp}_2}$); 3. the position corresponding to a given p, p_r and μ_p . The z values of these points are $z_{\text{ini}}, z_{\text{tp}_1}$ and z_{tp_2} , and z_p . The former three ones can be evaluated from $z(r)$ functions given in the right column of Table 3. z_p can be evaluated from function $z = \wp(p \pm \Pi_r; g_2, g_3)$ for cases 1, 4, 5 and $z = \text{sn}(s\sqrt{\lambda_1(1 - m^2)}p \pm \Pi_r|k^2)$ for case 2, and $z = \text{sn}(s\sqrt{\lambda_2(1 - m^2)}p \pm \Pi_r|k^2)$ for case 3 (for μ, z_p can be computed from $z = \wp(p \pm \Pi_\mu; g_2, g_3)$). It is

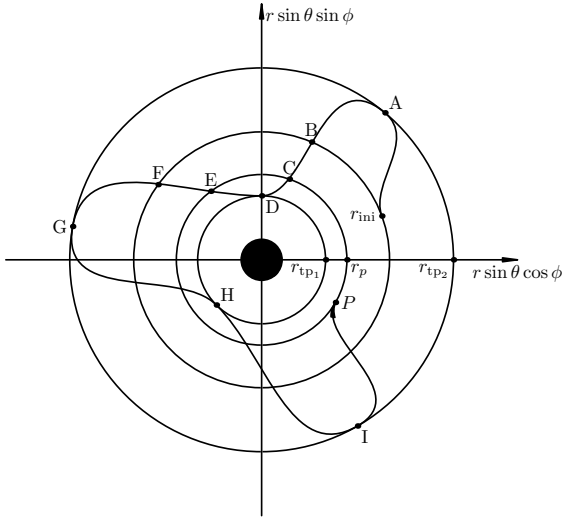


Fig. 1. The motion of r illustrated schematically. It has been projected onto the equatorial plane of the black hole. r_{tp_1} and r_{tp_2} are radial turning points, in which the motion is confined. Point P indicates the position for a given p . The whole integral path is not monotonous, and should be divided into several sections, each one has the maximum proper length. Such as DA, DG, HG, HI, PI. From the definitions of $I_{0\alpha r}$, $I_{1\alpha r}$, and $I_{2\alpha r}$ (see text), one has $I_{0\alpha r} = \int_B^C = \int_F^E$, $I_{1\alpha r} = \int_C^D = \int_E^D$, $I_{2\alpha r} = \int_A^C = \int_G^E$, $IT_{1\alpha r} = \int_B^D = \int_F^D$, and $IT_{2\alpha r} = \int_A^B = \int_G^F$, etc..

noted that the functions $z(r)$ are monotonously decreasing, we have $z_{tp_1} \geq z_{ini} \geq z_{tp_2}$ and $z_{tp_1} \geq z_p \geq z_{tp_2}$ (for μ , since the function $z(\mu)$ given in Table 1. is monotonously increasing, the two relationships are still valid).

In addition to z_p , for a given p , we can also obtain the number of times that the particle meets the two turning points. We assume that the particle meets r_{tp_1} (or μ_{tp_1}) for Nt_1 times, and r_{tp_2} (or μ_{tp_2}) for Nt_2 times. Nt_1 or Nt_2 is zero if r_{tp_1} or r_{tp_2} does not exist. To get Nt_1 and Nt_2 for a given p , we define the following five integrals with the help of Table 4:

$$\begin{aligned} p_0 &= \int_{z_{ini}}^{z_p} W(z) dz, & p_1 &= \int_{z_p}^{z_{tp_1}} W(z) dz, & p_2 &= \int_{z_{tp_2}}^{z_p} W(z) dz, \\ I_1 &= \int_{z_{ini}}^{z_{tp_1}} W(z) dz, & I_2 &= \int_{z_{tp_2}}^{z_{ini}} W(z) dz, \end{aligned} \quad (42)$$

where $W(z)$ represents the integrands in Table 4. Apparently we have $p_1 \geq 0$ and $p_2 \geq 0$, and

$$p_1 = I_1 - p_0, \quad p_2 = I_2 + p_0. \quad (43)$$

With the above definitions, we get the following identity

$$\begin{aligned} p &= -\text{sign}(p_\beta) p_0 + 2Nt_1 p_1 + 2Nt_2 p_2, \\ &= -[\text{sign}(p_\beta) + 2Nt_1 - 2Nt_2] p_0 + 2Nt_1 I_1 + 2Nt_2 I_2, \end{aligned} \quad (44)$$

where $\beta = r$ or θ , and p_β is the initial value of r or θ component of the four-momentum. One can get Nt_1 and Nt_2 from the above equations by trial and error, because Nt_1 and Nt_2 increase regularly as the particle moves, i.e., when $p_\beta > 0$ (or, $p_\beta = 0$ and $z_{ini} = z_{tp_1}$), Nt_1 and Nt_2 increase as:

$$\begin{aligned} Nt_1 &= 0, 0, 1, 1, 2, 2, 3, 3... \\ Nt_2 &= 0, 1, 1, 2, 2, 3, 3, 4... \end{aligned}$$

When $p_\beta < 0$ (or, $p_\beta = 0$ and $z_{ini} = z_{tp_2}$), Nt_1 and Nt_2 increase as:

$$\begin{aligned} Nt_1 &= 0, 1, 1, 2, 2, 3, 3, 4... \\ Nt_2 &= 0, 0, 1, 1, 2, 2, 3, 3... \end{aligned}$$

Note the path and limits of integrals in t , ϕ and σ are exactly the same with those of p . We introduce the following definitions:

$$\begin{aligned} I_{0\alpha\beta} &= \int_{z_{ini}}^{z_p} F_\beta(z) dz, & I_{1\alpha\beta} &= \int_{z_p}^{z_{tp_1}} F_\beta(z) dz, & I_{2\alpha\beta} &= \int_{z_{tp_2}}^{z_p} F_\beta(z) dz, \\ IT_{1\alpha\beta} &= \int_{z_{ini}}^{z_{tp_1}} F_\beta(z) dz, & IT_{2\alpha\beta} &= \int_{z_{tp_2}}^{z_{ini}} F_\beta(z) dz. \end{aligned} \quad (45)$$

where $\alpha = t, \phi, \sigma$. Similarly we have

$$I_{1\alpha\beta} = IT_{1\alpha\beta} - I_{0\alpha\beta}, \quad I_{2\alpha\beta} = IT_{2\alpha\beta} + I_{0\alpha\beta}. \quad (46)$$

Then the integrals in t, ϕ and σ can be written as

$$\begin{aligned} I_{\alpha\beta} &= -\text{sign}(p_\beta) I_{0\alpha\beta} + 2Nt_1 I_{1\alpha\beta} + 2Nt_2 I_{2\alpha\beta}, \\ &= -[\text{sign}(p_\beta) + 2Nt_1 - 2Nt_2] I_{0\alpha\beta} + 2Nt_1 IT_{1\alpha\beta} + 2Nt_2 IT_{2\alpha\beta}. \end{aligned} \quad (47)$$

Finally we have

$$t = I_{tr} + I_{t\theta}, \quad \phi = I_{\phi r} + I_{\phi\theta}, \quad \sigma = I_{\sigma t} + I_{\sigma\theta}. \quad (48)$$

3.3.2. The computation of elliptic integrals by Carlson's approach

In this section we discuss how to compute the elliptic integrals appeared in t, ϕ and σ by Carlson's approach. Firstly, we reduce these integrals to the standard forms. Before the reductions we introduce two notations $J_k(h)$ and $I_k(h)$ with the following definition:

$$J_k(h) = \int_y^x \frac{dt}{(t-h)^k \sqrt{4t^3 - g_2 t - g_3}}, \quad (49)$$

$$I_k(h) = \int_y^x \frac{dr}{(r-h)^k \sqrt{[(r-u)^2 + v^2][(r-w)^2 + s^2]}}, \quad (50)$$

where $k = -2, -1, 0, 1, 2$. From Equations (13)-(15), we have

$$\sigma_\mu = t_\mu = a^2 \left[\frac{b_0^2}{16} J_2\left(\frac{b_1}{4}\right) + \frac{b_0 \mu_{tp_1}}{2} J_1\left(\frac{b_1}{4}\right) + \mu_{tp_1}^2 p \right], \quad (51)$$

$$\phi_\mu = \lambda \left[\frac{p}{1 - \mu_{tp_1}^2} - \frac{C_-}{2} J_1(z_-) + \frac{C_+}{2} J_1(z_+) \right], \quad (52)$$

where

$$C_\pm = \frac{b_0}{4(\pm 1 - \mu_{tp_1})^2}, \quad (53)$$

$$z_\pm = \frac{b_0}{4} \frac{1}{(\pm 1 - \mu_{tp_1})} + \frac{b_1}{4}. \quad (54)$$

Noting the definition of parameter p , we have replaced J_0 by p in the above equations.

The reduced standard forms of integrals for r are given in Table 5 and 6. The standard forms for the special cases, such as the equatorial plane motion and the spherical motion, can be obtained directly and not given here anymore.

Carlson (1988, 1989, 1991, 1992) developed a new approach to compute elliptic integrals (Press et al. 2007). He gave new

Table 5. Standard forms of integrals

Case	σ_r, t_r, ϕ_r
1	$\sigma_r = \frac{b_0^2}{16} J_2\left(\frac{b_1}{4}\right) + \frac{b_0 r_{\text{tp}1}}{2} J_1\left(\frac{b_1}{4}\right) + r_{\text{tp}1}^2 p, \quad (55)$
	$t_r = \sigma_r + \left[(2 + e\varepsilon)(2 + r_{\text{tp}1}) - e^2 + A_{t+} - A_{t-} \right] p + \frac{(2 + e\varepsilon)b_0}{4} J_1\left(\frac{b_1}{4}\right) - D_{t+} J_1(z_+) + D_{t-} J_1(z_-), \quad (56)$
	$\phi_r = a \left[(A_{\phi+} - A_{\phi-}) p - D_{\phi+} J_1(z_+) + D_{\phi-} J_1(z_-) \right]. \quad (57)$
2, 3	$\sigma_r = \frac{1}{\sqrt{ 1 - m^2 }} I_{-2}(0), \quad (58)$
	$t_r = \sigma_r + \frac{1}{\sqrt{ 1 - m^2 }} \left[(2 + e\varepsilon) I_{-1}(0) + [2(2 + e\varepsilon) - e^2] p + B_{t+} I_1(r_+) - B_{t-} I_1(r_-) \right], \quad (59)$
	$\phi_r = \frac{a}{\sqrt{ 1 - m^2 }} \left[B_{\phi+} I_1(r_+) - B_{\phi-} I_1(r_-) \right]. \quad (60)$
4, 5	$\sigma_r = \frac{16}{b_0^2} J_{-2}(0) - \frac{8b_1}{b_0^2} J_{-1}(0) + b_1^2 J_0(0), \quad (61)$
	$t_r = \sigma_r + \frac{4}{b_0} (2 + e\varepsilon) J_{-1}(0) + \left[(2 + e\varepsilon) \left(2 - \frac{b_1}{b_0} \right) - e^2 \right] p + \frac{b_0}{4} [B_{t+} J_1(\tilde{z}_+) - B_{t-} J_1(\tilde{z}_-)], \quad (62)$
	$\phi_r = \frac{ab_0}{4} [B_{\phi+} J_1(\tilde{z}_+) - B_{\phi-} J_1(\tilde{z}_-)]. \quad (63)$

Table 6. Definitions of Table 5.

Case	Definitions
1	$r_{\pm} = 1 \pm \sqrt{1 - a^2 - e^2}, \quad z_{\pm} = \frac{b_0}{4(r_{\pm} - r_{\text{tp}1})} + \frac{b_1}{4},$ $A_{t\pm} = \frac{k_1 r_{\pm} + k_2}{(r_+ - r_-)(r_{\text{tp}1} - r_{\pm})}, \quad D_{t\pm} = \frac{(k_1 r_{\pm} + k_2) b_0}{4(r_+ - r_-)(r_{\text{tp}1} - r_{\pm})^2},$ $k_1 = 8 - 2a\lambda + 4(e\varepsilon - e^2) - e^3 \varepsilon,$ $k_2 = e^2(e^2 + a\lambda) - 2(a^2 + e^2)(2 + e\varepsilon),$ $A_{\phi\pm} = \frac{(2 - e\varepsilon)r_{\pm} - (e^2 + a\lambda)}{(r_+ - r_-)(r_{\text{tp}1} - r_{\pm})},$ $D_{\phi\pm} = \frac{(2 - e\varepsilon)r_{\pm} - (e^2 + a\lambda)}{4(r_+ - r_-)(r_{\text{tp}1} - r_{\pm})^2} b_0.$
2, 3	$B_{t\pm} = \frac{k_1 r_{\pm} + k_2}{r_+ - r_-}, \quad B_{\phi\pm} = \frac{(2 - e\varepsilon)r_{\pm} - (e^2 + a\lambda)}{r_+ - r_-}.$
4, 5	$\tilde{z}_{\pm} = \frac{b_0}{4} r_{\pm} + \frac{b_1}{4}.$

definitions of the standard elliptic integrals of the first and third kinds

$$R_F(x, y, z) = \frac{1}{2} \int_0^{\infty} \frac{dt}{\sqrt{(t+x)(t+y)(t+z)}}, \quad (64)$$

$$R_J(x, y, z, p) = \frac{3}{2} \int_0^{\infty} \frac{dt}{(t+p) \sqrt{(t+x)(t+y)(t+z)}}, \quad (65)$$

and the degenerate cases of $R_C(x, y) = R_F(x, y, y)$ and $R_D(x, y, z) = R_J(x, y, z, z)$. R_D can be regarded as the standard elliptic integral of the second kind. Carlson denotes the elliptic integrals by a symbol with the following definition:

$$[p_1, \dots, p_k] = \int_y^x \prod_{i=1}^k (a_i + b_i t)^{p_i/2} dt. \quad (66)$$

If $a_i + b_i t$ is complex, then its complex conjugate $\overline{a_i + b_i t}$ must exist and guarantee the integral to be real. And $(a_i + b_i t)(\overline{a_i + b_i t}) = f + gt + ht^2$. Thus

$$[p_1, p_1, p_3, \dots, p_k] = \int_y^x (f + gt + ht^2)^{p_1/2} \times \prod_{j=3}^k (a_j + b_j t)^{p_j/2} dt. \quad (67)$$

For a particular elliptic integral, there is an unique formula to evaluate it. We give a simple example here:

$$[-1, -1, -1, -1] = 2R_F(U_{12}^2, U_{13}^2, U_{14}^2), \quad (68)$$

where

$$U_{ij} = (X_i X_j Y_k Y_m + Y_i Y_j X_k X_m) / (x - y),$$

$$X_i = \sqrt{a_i + b_i x}, \quad Y_i = \sqrt{a_i + b_i y}.$$

The elliptic integrals need to be evaluated in this paper are: $J_1, J_2, I_2, I_{-1}, I_{-2}$, which can be recast by Carlson's notations. When equation $4t^3 - g_2 t - g_3 = 0$ has three real roots denoted by e_1, e_2, e_3 , one has (Carlson 1988)

$$J_k(h) = s_h \frac{1}{2} \int_y^x \frac{dt}{\sqrt{(t-e_1)(t-e_2)(t-e_3)(t-h)^{2k}}} \\ = s_h \frac{1}{2} [-1, -1, -1, -2k], \quad (69)$$

where $s_h = \text{sign}[(y-h)^k]$. When equation $4t^3 - g_2 t - g_3 = 0$ has one pair of complex roots and one real root e_1 , one has (Carlson 1991)

$$J_k(h) = s_h \frac{1}{2} \int_y^x \frac{dt}{\sqrt{(t-e_1)(t^2 + gt + f)(t-h)^{2k}}} \\ = s_h \frac{1}{2} [-1, -1, -1, -2k]. \quad (70)$$

$I_k(h)$ corresponds to the case that equation $R_r(r) = 0$ has no real roots and can be expressed as (Carlson 1992):

$$I_k(h) = s_h \int_y^x \frac{dr}{\sqrt{[(r-u)^2 + v^2][(r-w)^2 + s^2](r-h)^{2k}}}, \quad (71) \\ = s_h [-1, -1, -1, -1, -2k].$$

Up to now, we have expressed all coordinates and proper time as functions of parameter p semi-analytically. As discussed in Yang & Wang (2013), such treatment is very convenient for massive particles whose geodesics can be bounded, and the number of times that the particle meets the turning points can be arbitrary both for r and μ coordinates. In addition to p , one needs to prescribe the constants of motion. In the next section we discuss how to get them from the initial four-momentum of a particle.

4. The constants of motion

As mentioned above, the constants of motion throughout this paper are defined as

$$\lambda = \frac{L}{E}, \quad q = \frac{Q}{E^2}, \quad m = \frac{\mu_m}{E}, \quad \varepsilon = \frac{\epsilon}{E}, \quad (72)$$

which can be gotten from the initial four-momentum of a particle given in a locally nonrotating frame (LNRF) reference. But to

handle more complicated applications, we want to specify the initial four-momentum in the reference of an assumed emitter, instead of an LNRF reference directly. However the initial four-momentum is finally transformed into an LNRF reference by a Lorentz transformation.

Now we introduce the LNRF reference, which is also called as zero angular momentum observers (ZAMO) (Bardeen et al. 1972). The orthonormal tetrad is given by

$$\mathbf{e}_{(a)}(\text{LNRF}) = e_{(a)}^{\nu} \partial_{\nu}, \quad (73)$$

where

$$e_{(a)}^{\nu} = \begin{pmatrix} e^{-\nu} & 0 & 0 & \omega e^{-\nu} \\ 0 & e^{-\mu_1} & 0 & 0 \\ 0 & 0 & e^{-\mu_2} & 0 \\ 0 & 0 & 0 & e^{-\psi} \end{pmatrix}, \quad (74)$$

and the dual form of which is

$$\mathbf{e}^{(a)}(\text{LNRF}) = e_{\nu}^{(a)} dx^{\nu}, \quad (75)$$

where

$$e_{\nu}^{(a)} = \begin{pmatrix} e^{\nu} & 0 & 0 & 0 \\ 0 & e^{\mu_1} & 0 & 0 \\ 0 & 0 & e^{\mu_2} & 0 \\ -\omega e^{\psi} & 0 & 0 & e^{\psi} \end{pmatrix}. \quad (76)$$

We assume that the particle is shotted by an emitter at the initial position, where the emitter has coordinate velocities $\dot{r} = dr/dt$, $\dot{\theta} = d\theta/dt$, and $\dot{\phi} = \Omega = d\phi/dt$, then its physical velocities $v_r, v_{\theta}, v_{\phi}$ with respect to the LNRF fixed at the same point can be written as (Bardeen et al. 1972):

$$v_r = e^{\mu_1 - \nu} \dot{r}, \quad v_{\theta} = e^{\mu_2 - \nu} \dot{\theta}, \quad v_{\phi} = e^{\psi - \nu} (\Omega - \omega). \quad (77)$$

The orthonormal tetrad of the emitter can be obtained by rotating the tetrad of the LNRF reference in the local four dimension spacetime. The rotation is nothing but a Lorentz transformation. We denote the matrix of the rotation by Λ , and have

$$\mathbf{e}_{(a)}(\text{em}) = \Lambda_{(a)}^{(b)} \mathbf{e}_{(b)}(\text{LNRF}), \quad (78)$$

where (Misner et al. 1973)

$$\Lambda_{(a)}^{(b)} = \begin{pmatrix} \gamma & \gamma v_r & \gamma v_{\theta} & \gamma v_{\phi} \\ \gamma v_r & 1 + \gamma^2 v_r^2 / (1 + \gamma) & \gamma^2 v_r v_{\theta} / (1 + \gamma) & \gamma^2 v_r v_{\phi} / (1 + \gamma) \\ \gamma v_{\theta} & \gamma^2 v_{\theta} v_r / (1 + \gamma) & 1 + \gamma^2 v_{\theta}^2 / (1 + \gamma) & \gamma^2 v_{\theta} v_{\phi} / (1 + \gamma) \\ \gamma v_{\phi} & \gamma^2 v_{\phi} v_r / (1 + \gamma) & \gamma^2 v_{\phi} v_{\theta} / (1 + \gamma) & 1 + \gamma^2 v_{\phi}^2 / (1 + \gamma) \end{pmatrix}, \quad (79)$$

where $\gamma = [1 - (v_r^2 + v_{\theta}^2 + v_{\phi}^2)]^{-1/2}$, and the covariant tetrad of the emitter is

$$\mathbf{e}^{(a)}(\text{em}) = (\Lambda^{-1})_{(a)}^{(b)} \mathbf{e}^{(b)}(\text{LNRF}), \quad (80)$$

where

$$(\Lambda^{-1})_{(a)}^{(b)} = \begin{pmatrix} \gamma & -\gamma v_r & -\gamma v_{\theta} & -\gamma v_{\phi} \\ -\gamma v_r & 1 + \gamma^2 v_r^2 / (1 + \gamma) & \gamma^2 v_r v_{\theta} / (1 + \gamma) & \gamma^2 v_r v_{\phi} / (1 + \gamma) \\ -\gamma v_{\theta} & \gamma^2 v_{\theta} v_r / (1 + \gamma) & 1 + \gamma^2 v_{\theta}^2 / (1 + \gamma) & \gamma^2 v_{\theta} v_{\phi} / (1 + \gamma) \\ -\gamma v_{\phi} & \gamma^2 v_{\phi} v_r / (1 + \gamma) & \gamma^2 v_{\phi} v_{\theta} / (1 + \gamma) & 1 + \gamma^2 v_{\phi}^2 / (1 + \gamma) \end{pmatrix}. \quad (81)$$

Equivalently, one has

$$\mathbf{e}_{(a)}(\text{LNRF}) = (\Lambda^{-1})_{(a)}^{(b)} \mathbf{e}_{(b)}(\text{em}), \quad (82)$$

$$\mathbf{e}^{(a)}(\text{LNRF}) = (\Lambda)_{(b)}^{(a)} \mathbf{e}^{(b)}(\text{em}). \quad (83)$$

In the rest frame of the emitter, the components of four-momentum of the particle are denoted by $p'_{(a)}$, which can be regarded as the projections of the momentum \mathbf{p} on the corresponding basis vectors, i.e.,

$$p'_{(a)} = \mathbf{p} \cdot \mathbf{e}_{(a)}(\text{em}). \quad (84)$$

Multiplying both sides of Equation (82) by \mathbf{p} , we get

$$e_{(a)}^{\nu} p_{\nu} = (\Lambda^{-1})_{(a)}^{(b)} p'_{(b)}, \quad (85)$$

Assuming that the physical velocities of the particle with respect to the emitter are: $v'_r, v'_{\theta}, v'_{\phi}$, we have

$$p'_{(a)} = \gamma' \mu_m (-1, v'_r, v'_{\theta}, v'_{\phi}), \quad (86)$$

where $\gamma' = [1 - (v_r'^2 + v_{\theta}'^2 + v_{\phi}'^2)]^{-1/2}$ is the Lorentz factor. Equation (85) can be expanded explicitly by using Equations (11) and (74):

$$E e^{-\nu} (1 - \lambda \omega) = \gamma' \mu_m k_{(t)}, \quad (87)$$

$$E e^{-\mu_1} s_r \frac{\sqrt{R_r}}{\Delta} = \gamma' \mu_m k_{(r)}, \quad (88)$$

$$E e^{-\mu_2} s_{\theta} \sqrt{\Theta_{\theta}} = \gamma' \mu_m k_{(\theta)}, \quad (89)$$

$$E \lambda e^{-\psi} = \gamma' \mu_m k_{(\phi)}, \quad (90)$$

where

$$k_{(t)} = \gamma (1 + \mathbf{v} \cdot \mathbf{v}'), \quad (91)$$

$$k_{(r)} = \gamma v_r + v'_r + \frac{\gamma^2 v_r}{1 + \gamma} \mathbf{v} \cdot \mathbf{v}', \quad (92)$$

$$k_{(\theta)} = \gamma v_{\theta} + v'_{\theta} + \frac{\gamma^2 v_{\theta}}{1 + \gamma} \mathbf{v} \cdot \mathbf{v}', \quad (93)$$

$$k_{(\phi)} = \gamma v_{\phi} + v'_{\phi} + \frac{\gamma^2 v_{\phi}}{1 + \gamma} \mathbf{v} \cdot \mathbf{v}', \quad (94)$$

$$\mathbf{v} \cdot \mathbf{v}' = v_r v'_r + v_{\theta} v'_{\theta} + v_{\phi} v'_{\phi}. \quad (95)$$

Solve Equations (87) and (90) for λ , we get

$$\lambda = \frac{k_{(\phi)} \sin \theta}{k_{(t)} \sqrt{\Delta} \Sigma / A + k_{(\phi)} \omega \sin \theta}. \quad (96)$$

With λ , from Equation (87), we get

$$m = \frac{e^{-\nu}}{\gamma' k_{(t)}} (1 - \lambda \omega). \quad (97)$$

With λ and m , from Equation (89), we get

$$q = \left[\left(\frac{k_{(\phi)}}{k_{(t)} \sqrt{\Delta} \Sigma / A + k_{(\phi)} \omega \sin \theta} \right)^2 + a^2 (m^2 - 1) \right] \cos^2 \theta + m^2 \Sigma \gamma'^2 k_{(\theta)}^2. \quad (98)$$

With λ , m , and q , from Equation (88), we get a quadratic equation for ε ,

$$a_1 \varepsilon^2 + b_1 \varepsilon + c_1 = 0, \quad (99)$$

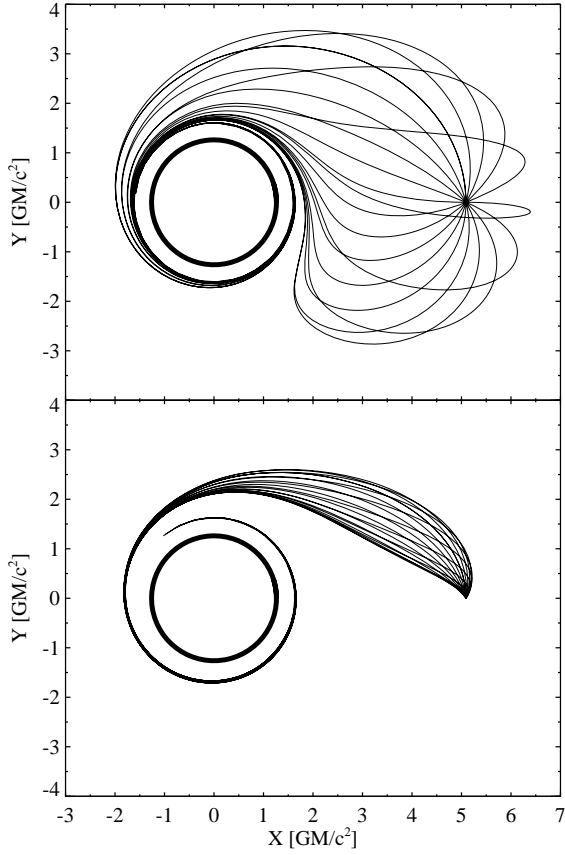


Fig. 2. This figure shows the trajectories of a set of particles, which are confined in the equatorial plane and do plane motions. The spin and electric charge of the black hole are 0.96 and 0.1 respectively. The electric charges of particles are ε_+ (top panel) and ε_- (bottom panel). The initial physical speed of the particles is isotropical and equal to 0.35 with respect to the LNRF. The initial coordinates of the particles are $r = 5 r_g$, $\theta = 90^\circ$, and $\phi = 0$. A circle at the center represents the event horizon.

where

$$a_1 = e^2 r^2, \quad (100)$$

$$b_1 = 2er(r^2 + a^2 - a\lambda), \quad (101)$$

$$c_1 = (1 - m^2)r^4 + 2m^2 r^3 - [q + \lambda^2 + a^2(m^2 - 1) + e^2 m^2]r^2 + 2[q + (a - \lambda)^2]r - e^2(a - \lambda)^2 - (a^2 + e^2)q - \Delta \Sigma (m\gamma' k_{(r)})^2. \quad (102)$$

We then get two values,

$$\varepsilon_{\pm} = \frac{-b_1 \pm \sqrt{b_1^2 - 4a_1 c_1}}{2a_1}, \quad (103)$$

where ε_+ represents positive electric charge, and ε_- represents negative electric charge. In Figure 2, we plot a set of geodesic orbits of particles emitted isotropically in an LNRF reference. These particles are confined in the equatorial plane. The particles have ε_+ in the top panel, and ε_- in the bottom panel.

5. A brief introduction to the code

According to the discussions above, we have developed a new public code for computing null and time-like geodesics in a

K-N spacetime². We name the code *ynogkm*, which is written in fortran 95, and the object oriented method is used. The code consists of several independent modules, in which each one completes a special goal. The most important two modules are *ellfunction* and *blcoordinates*. The former one contains the supporting functions and subroutines computing elliptic integrals by Carlson's approach. The latter one contains the functions and routines computing the B-L coordinate functions: $r(p)$, $\mu(p)$, $\phi(p)$, and $t(p)$, as well as proper time function $\sigma(p)$. In *blcoordinates*, we provide a subroutine named *ynogkm* to compute all coordinates and proper times simultaneously for a given p . We also provide two functions named *radiusm* and *mucosm* to compute $r(p)$ and $\mu(p)$ respectively. In an axis-symmetry case, one only needs to compute r and μ .

Before calling these functions and subroutines to compute the B-L coordinates, one needs to provide the constants of motion, namely, λ , q , m , and ε . As discussed in the above section, we have provided a set of formulae to compute these constants from v'_i , which are the physical velocities of the particle with respect to an assumed emitter, who has also physical velocities v_i with respect to an LNRF reference. According to these formulae, we provide a subroutine named *lambdaqm* to calculate λ , q , m , ε , and $k_{(a)}$ defined by Equations (91)-(94). Except for a factor $\gamma'\mu_m$, $k_{(a)}$ actually are exactly equal to the initial four-momentum of the test particle given in an LNRF. Thus $k_{(a)}$ can be used to determine the signs in front of Π_r or Π_μ . The other initial parameters need to be specified are included: (1) the initial coordinates of the particle, r_{ini} , θ_{ini} , ϕ_{ini} and t_{ini} . The latter two ones are usually set to be zero; (2) the physical velocities of the assumed emitter with respect to an LNRF, v_r , v_θ , and v_ϕ ; (3) the physical velocities of the particle with respect to the assumed emitter, v'_r , v'_θ , and v'_ϕ ; (4) the spin parameter a and the electric charge e of the black hole. With a given p and those initial parameters, one can do the calculations directly without giving the number of times that the particle meets the two turning points, namely Nt_1 and Nt_2 .

In our code the parameter p is an independent variable, which is always positive and monotonously increasing along a particular geodesic. When the geodesic is unbounded, it has a termination, either at infinity or the event horizon. The value of p corresponding to the termination is a finite number, denoted by p_{max} . We provide a subroutine named *ptotal* to calculate this number. Apparently, when a p given by the user is bigger than p_{max} , it has no meaning and the code resets it to be p_{max} mandatorily. When a geodesic is bounded, its termination does not exist at all and p can take any positive value.

For a more detailed introduction, one can see the README³ file. In the next section, we give the results of our code for toy problems.

6. Applications for toy problems

To show the utility of our code, we apply it to toy problems. The results for five such examples are illustrated in this section.

6.1. Geodesic orbits of massive particles

The most important application of the code is to compute the geodesics of massive particles in a K-N spacetime. As the first application, we use the code to compute the orbits of a set of

² The source FORTRAN code can be download on our Web site <http://www1.ynao.ac.cn/~yangxl/yxl.html>

³ <http://www1.ynao.ac.cn/~yangxl/ynogkm/readme.pdf>

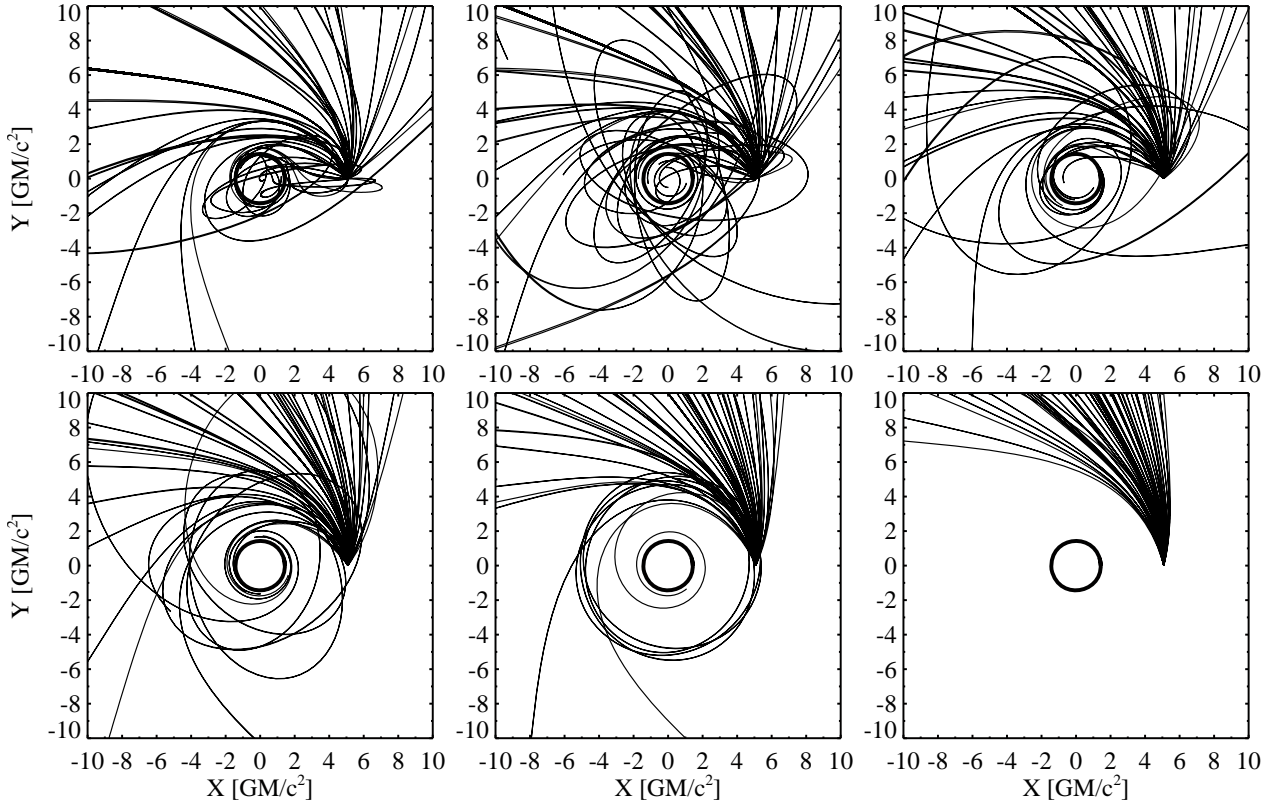


Fig. 3. A set of geodesics of massive particles orbit around a black hole with $a=0.9$. The physical velocities of the emitter with respect to the LNRF are $v_r = 0$, $v_\theta = 0$, and $v_\phi = 0.4$, $v_\phi = 0.5$, $v_\phi = 0.6$, $v_\phi = 0.7$, $v_\phi = 0.8$, $v_\phi = 0.9$ for panels from left to right, top to bottom. The velocities of these particles are specified isotropically in the rest frame of the emitter and $v'_{pt} = 0.6$.

test particles that are emitted isotropically in the local rest frame of an assumed emitter. The particles have a constant speed v'_{pt} but different directions in the local reference, and $v'_{pt} = 0.6$. The orientation of the velocity is described by ϑ and φ , thus the components of the velocity under the reference of the emitter are

$$v'_r = v'_{pt} \sin \vartheta \cos \varphi, \quad (104)$$

$$v'_\theta = v'_{pt} \sin \vartheta \sin \varphi, \quad (105)$$

$$v'_\phi = v'_{pt} \cos \vartheta. \quad (106)$$

The physical velocities of the emitter with respect to the LNRF reference are $v_r = 0$, $v_\theta = 0$, in which only the ϕ component is not zero and takes different values. We demonstrate the results in Figure 3. It is shown that as the speed of emitter increases, more particles become unbounded, and the beaming effect becomes more significant.

6.2. The orbits of spherical motion

The circular orbits in the Kerr spacetime has significant applications in the standard geometrically thin accretion disk systems. A particle in the accretion flow loses its angular momentum by viscosity and moves inward slowly. Its angular velocity is far greater than its radial velocity. Thus the particle moves in a circular orbit is a good approximation. The inner radius of the disk is usually located at the ISCO. Based on this assumption, one can measure the black hole spin by fitting the line profiles or the continuous spectra. Actually the circular orbits, in which the

particle is confined in the equatorial plane of the black hole, can be regarded as a special case of the spherical orbit. The radial velocity and acceleration of the particle in a spherical orbit are vanished, leading to two conditions: $dr/d\tau = 0$ and $d^2r/d\tau^2 = 0$. Using equation (4), these conditions reduce to (Bardeen et al. 1972; Wilkins 1972):

$$R_r = 0, \quad \frac{dR_r}{dr} = 0. \quad (107)$$

We use θ_* to denote the coordinate of one of the θ turning points, therefore we have $\Theta_\theta(\theta_*)=0$. Using the same strategy discussed in Shakura (1987), we can get the angular velocity of the particle at θ_*

$$\Omega^* = \frac{\sqrt{P}}{\sin \theta_* (\pm \Sigma \sqrt{r} + a \sin \theta_* \sqrt{P})}, \quad (108)$$

where $P = M(r^2 - a^2 \cos^2 \theta_*) - e^2 r$, and the constants of motion:

$$\frac{E}{\mu_m} = \frac{\pm a \sin \theta_* \sqrt{P} + (\Delta - a^2 \sin^2 \theta_*) \sqrt{r}}{\sqrt{\Sigma} \sqrt{-P + (\Delta - a^2 \sin^2 \theta_*) r \pm 2a \sin \theta_* \sqrt{rP}}}, \quad (109)$$

$$\frac{L}{\mu_m} = \frac{\sin \theta_* [\pm (r^2 + a^2) \sqrt{P} - \sqrt{r} a \sin \theta_* (2Mr - e^2)]}{\sqrt{\Sigma} \sqrt{-P + (\Delta - a^2 \sin^2 \theta_*) r \pm 2a \sin \theta_* \sqrt{rP}}}, \quad (110)$$

$$\begin{aligned} \frac{Q}{\mu_m^2} &= \cos^2 \theta_* \left[a^2 \left(1 - \frac{E^2}{\mu_m^2} \right) + \frac{1}{\sin^2 \theta_*} \frac{L^2}{\mu_m^2} \right], \\ &= \frac{r \cos^2 \theta_* [A_Q \mp 2a \sin \theta_* (2Mr - e^2) r \sqrt{rP}]}{\Sigma [-P + (\Delta - a^2 \sin^2 \theta_*) r \pm 2a \sin \theta_* \sqrt{rP}]}, \end{aligned} \quad (111)$$

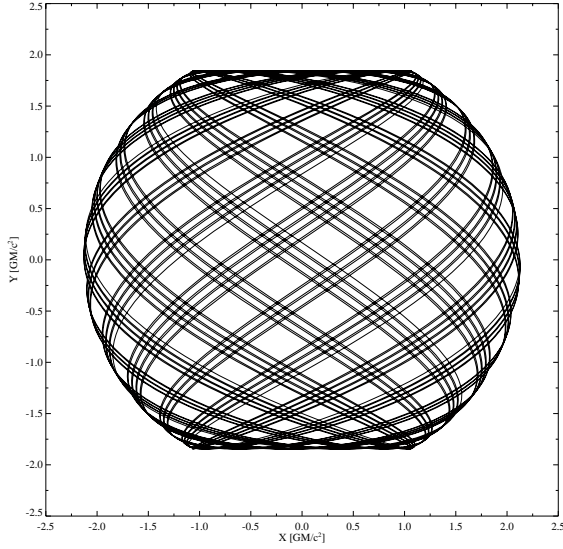


Fig. 4. The orbit of a particle in a spherical motion. The parameters are: the black hole spin $a=0.998$, the radius of the orbit $r=2 r_g$, the turning point $\theta_* = 30^\circ$, the inclination angle of the observer $\theta_{\text{obs}} = 90^\circ$.

where

$$A_Q = (r^2 + a^2)^2(Mr - e^2) + a^2\{[Mr(r^2 - a^2) + e^2 a^2] \sin^2 \theta_* - (2Mr - e^2)^2 \cos^2 \theta_*\}. \quad (112)$$

In these formulae, the upper sign refers to the prograde orbits (i.e., corotating with $L>0$), while the lower sign refers to retrograde orbits (counter rotating with $L<0$).

In Figure 4, we plot the orbit of a particle in a spherical motion. Given the parameters: a, e, r , and θ_* , from Equations (109)-(111), we can get the constants of motion: λ, q, m , with which from equation $R_r = 0$ (or $dR_r/dr = 0$), we can get the final constant ε . For simplicity, we let both e and ε to be zero in this figure. Comparing with circular motion, the most significant effect of spherical motion is the precession of the orbit.

Correspondingly, the spherical motion has also three kinds of marginal orbits, which are:

(1). Photon orbit r_{ph} , which is the innermost boundary of the spherical orbits for particles, it occurs when the denominator of Equations (109), (110), and (111) vanishes, i.e.,

$$-P + (\Delta - a^2 \sin^2 \theta_*)r \pm 2a \sin \theta_* \sqrt{rP} = 0. \quad (113)$$

(2). Marginally bound spherical orbit r_{mb} , which occurs when $E/\mu_m = 1$.

(3). Inner most marginally stable spherical orbit r_{ms} (ISSO). The stable condition requires that $d^2 R_r/dr^2 \leq 0$, which yields the equivalent condition,

$$1 - \left. \left(\frac{E}{\mu_m} \right)^2 \right|_{e=0} \geq \frac{2Mr(r^2 - 3a^2 \cos^2 \theta_*)}{3r^4 - a^4 \cos^4 \theta_* - 6r^2 a^2 \cos^2 \theta_*}, \quad (114)$$

or $r \geq r_{\text{ms}}$. For simplicity we have let e to be zero in the above equation. If $\theta_* = \pi/2$, namely the circular orbits, this condition reduces to the same form of Equation (2.20) of Bardeen et al. (1972).

In our code, we provide three functions named $r_{\text{ms}}, r_{\text{mb}}$, and r_{ph} to compute the radii of these orbits with given a, θ_*, e . In Figure 5, we plot the radii of inner most stable spherical orbits

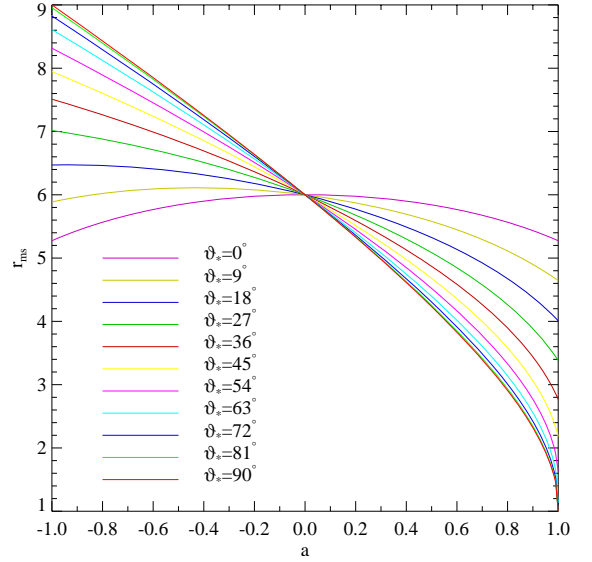


Fig. 5. The radii of the innermost stable orbits for the spherical motion around a Kerr black hole, as functions of the specific angular momentum a of the black hole.

as functions of a for various θ_* . For simplicity we let also $e = 0$ in this Figures. One can see that as θ_* increases, the radii become larger for $a > 0$ and smaller for $a < 0$. For $a = 0$, the radii keeps unchanged. When $\theta_* = 0^\circ$, the curve becomes symmetry for $a > 0$ and $a < 0$. The similar properties can be obtained for the radii of photon orbits and marginally bound orbits.

6.3. Orbits inside r_{ms}

The region inside ISSO usually called as the plug region, in which a particle moves along geodesics with constants of motion of the marginally stable spherical geodesic (Cunningham 1975) when its initial radial perturbation velocity $v_r = 0$. With the results presented in the above section, we get the constants of motion for the marginally stable spherical orbits

$$\left(\frac{E}{\mu_m} \right)^2 = 1 - \frac{2Mr_{\text{ms}}(r_{\text{ms}}^2 - 3a^2 \cos^2 \theta_*)}{D_{\text{ms}}}, \quad (115)$$

$$\left(\frac{L}{\mu_m} \right)^2 = 2Mr_{\text{ms}} \sin^2 \theta_* [3r_{\text{ms}}^4 - r_{\text{ms}}^2 a^2 (1 + \cos^2 \theta_*) + 3a^4 \cos^2 \theta_*] / D_{\text{ms}}, \quad (116)$$

$$\frac{Q}{\mu_m^2} = \frac{2Mr_{\text{ms}}^3 \cos^2 \theta_* (3r_{\text{ms}}^2 - a^2 \cos^2 \theta_*)}{D_{\text{ms}}}, \quad (117)$$

$$D_{\text{ms}} = 3r_{\text{ms}}^4 - a^4 \cos^4 \theta_* - 6r_{\text{ms}}^2 a^2 \cos^2 \theta_*, \quad (118)$$

and

$$R_r = 2M(r_{\text{ms}} - r)^3 [rr_{\text{ms}}^3 - 3a^2 r_{\text{ms}} \cos^2 \theta_* (r_{\text{ms}} + r) + a^4 \cos^4 \theta_*] / D_{\text{ms}}, \quad (119)$$

$$\Theta_\mu = 2Mr_{\text{ms}} (\cos^2 \theta_* - \mu^2) [(3a^4 \cos^2 \theta_* - r_{\text{ms}}^2 a^2) \mu^2 - r_{\text{ms}}^2 a^2 \cos^2 \theta_* + 3r_{\text{ms}}^4] / D_{\text{ms}}. \quad (120)$$

From the above two equations, we know that both r_{ms} and θ_* are the turning points. With these expressions, we can get the constants of motion immediately to compute the geodesic orbits inside r_{ms} . In Figure 6, we plot such an orbit. We take $a = 0.998$

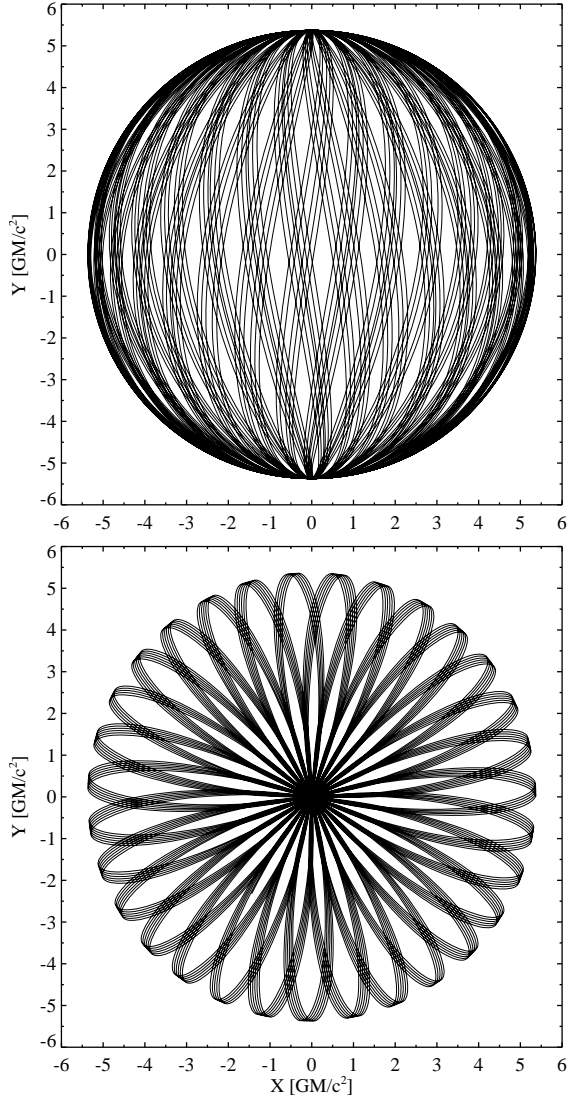


Fig. 6. The orbit of a particle moving inside the ISSO with the constants of motion of the ISSO. The black hole spin $a=0.998$ and the turning point $\theta_* = 0^\circ$. The radius of ISSO is $r = 5.2781 r_g$. The inclination angle $\theta_{\text{obs}} = 90^\circ$ for top panel and $\theta_{\text{obs}} = 0^\circ$ for bottom panel.

and $\theta_* = 0$, namely the particle goes through the spin axis of the black hole. Using the function $r_{\text{ms}}(a, \theta_*)$ in our code, we get $r_{\text{ms}} = 5.2781 r_g$. From this figure, one can see that the orbit is almost the same with a spherical motion, because the radial velocity is much smaller than the poloidal and azimuthal velocities.

6.4. The accretion flow of disk

Now we use our code to construct a toy model for mimicking accretion flows of skewed geometrically thin disks. The flows are composed by non-interacting particles, which fall freely into the black hole along the geodesic trajectories. It implies that we make a ballistic treatment to the fluid flow, and the dynamics and the structure of the disk are uniquely determined by the gravitational field of the black hole. It is also convenient to regard the accretion flow as a collection of test particles with same mass. The boundary conditions of the disk are assumed to be a ring at

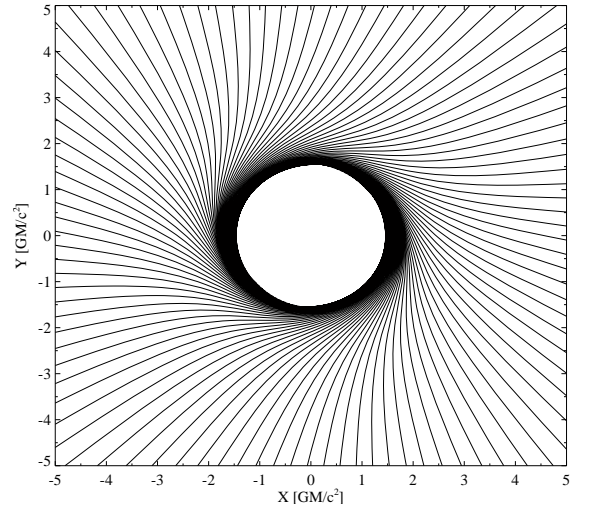


Fig. 7. The orbits of equal mass test particle flow inward to a black hole along geodesic trajectories, which form a smooth and curved surface. The black hole spin $a = 0.96$, the initial tilted angle of the disk is $\beta = 30^\circ$. The initial physical velocities of the particles under the tetrad are: $v'_x = 0.01$, $v'_y = 0.5$, $v'_z = -0.01 \cos \phi$. The radius of the ring is $20 r_g$.

$r = r_0$, from which the test particles are continuously injected. The plane of the ring has an inclination angle β with respect to the spin axis.

To describe the initial conditions of the test particles, namely the velocities, an orthonormal tetrad is established on the ring. We choose three spacial basis vectors of the tetrad as: $\mathbf{e}_x, \mathbf{e}_y, \mathbf{e}_z$, where \mathbf{e}_x is the tangent vector of the ring, \mathbf{e}_y is aligned along the radial direction and pointed inward, \mathbf{e}_z is the normal vector of the plane of the ring, and these vectors satisfy right-hand rule. In the local rest frame of the tetrad, the physical velocities of the particle are v'_x, v'_y, v'_z . According to the discussions in Section 4, in order to compute the constants of motion from these velocities, we need to transform them into the LNRF reference for getting v_r, v_θ, v_ϕ .

We denote the transformation matrix by $T(\theta, \phi, \beta)$. The explicit expression of T is presented in Appendix A. Hence we have $v_i = T_i^j v'_j$. Since the tetrad is attached on the ring, θ and ϕ are not independent variables, actually they satisfy the following equation

$$\sin \theta = \frac{\cos \beta}{\sqrt{1 - \sin^2 \phi \sin^2 \beta}}. \quad (121)$$

Therefore we have $v_i = T_i^j(\phi, \beta) v'_j$. Taking ϕ as an independent variable that varies from 0 to 2π , we can set the initial conditions for all test particles. In Figure 7, we plot such a set of geodesic orbits of test particles with same mass. The physical velocities are $v'_x = 0.01$, $v'_y = 0.5$, and $v'_z = -0.01$ respectively. From the figure, one can see that all trajectories form a smooth but curved surface.

Using the ray-tracing approach (Luminet 1979), we can image the curved surface. In Yang & Wang (2013), we have presented a new public code named ynogk to compute the null geodesics in a Kerr spacetime and a more general method to image a target object. The method requires one to provide the function describing the surface, i.e., $F(r, \theta, \phi) = 0$, or $F(x, y, z) = 0$. For this curved surface formed by geodesic orbits of test particles, we can not write out its explicit form, and only use the

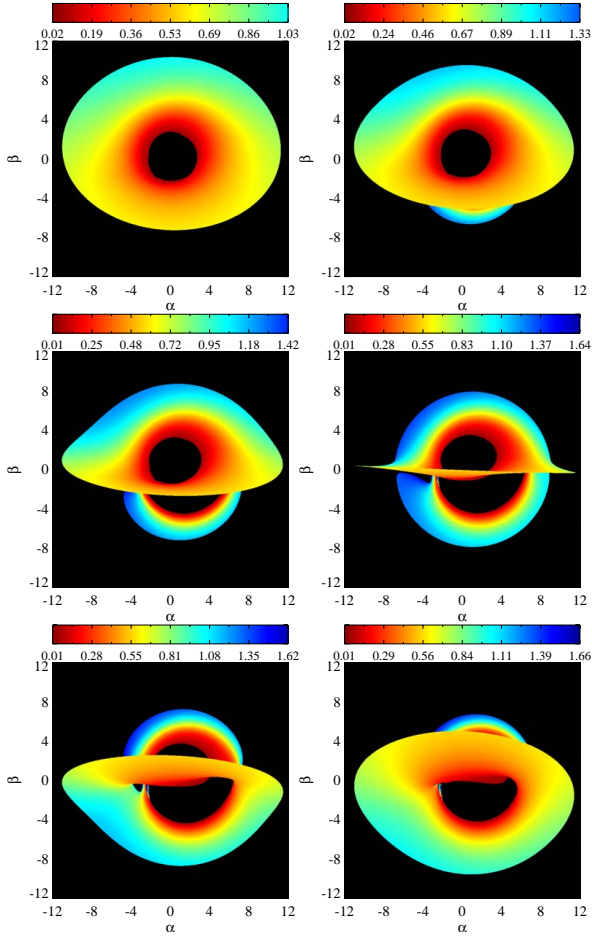


Fig. 8. The images of a skewed disk, whose inner and outer radii are $1.5 r_g$ and $10 r_g$. The parameters: $\beta = 30^\circ$, $\gamma_0 = 135^\circ$, black hole spin $a=0.998$, inclination angles θ_{obs} are 15° , 30° , 45° , 60° , 75° and 90° for panels a-f.

interpolation approach. To approximate the surface, we take N particles with N geodesic orbits. We take M points in each orbit, and totally get $N \times M$ points. We can get the coordinates of each point easily and write them as: $z_i = z_i(x_i, y_i)$. Using the interpolation approaches provided in Press et al. (2007), we can get a approximation function $z = z(x, y)$ that describes the surface.

In Figure 8, we plot the images of a skewed accretion disk that is composed by test particles falling freely into a black hole along geodesics viewed from different inclinations. The initial tilted angle of the disk is $\beta = 30^\circ$. Due to the frame drag effect, the particles drift into the black hole along spiral orbits, instead of a straight lines. The orbits make a gradual transition into the equatorial plane. The disk is significantly warped as moving inward. In the figure, the false color represent the redshift of emission coming from the disk surface. One can see that the approaching and receding sides of the disk are no longer the left and right sides, but the regions are farthest and nearest with respect to the observer respectively.

6.5. Stationary axisymmetric accretion flow

Tejeda et al. (2013) presented an analytic toy model to mimic the stationary axisymmetric accretion flow of a rotating cloud of non-interacting particles falling onto a Kerr black hole. In which the streamlines are described analytically in terms of timelike

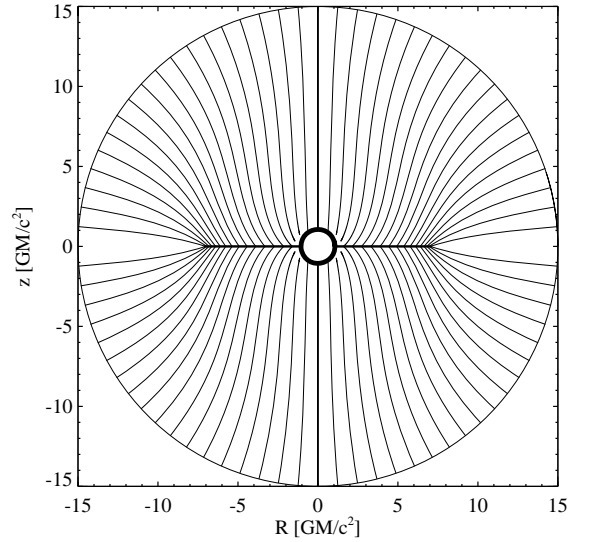


Fig. 9. Streamlines of axisymmetric accretion flow. Parameters are: black hole spin $a=0.998$; initial four velocities $u^r = 0.35$, $u^\theta = 0$, $u^\phi = -0.025$; radius of the shell $r_0 = 15 r_g$; $R = \sqrt{r^2 + a^2} \sin \theta$, $z = r \cos \theta$. The black circle and line represent the event horizon and accretion disk respectively. Compare to Figure 1. of Tejeda et al. (2013).

geodesics. Thus they solve the equations of motion with integral forms by elliptic functions. However their results are completely different comparing with ours. In addition, they just get the solutions for r and μ .

As a check of the validation of our code, we use it to mimic the similar accretion flow. Since the flow is axisymmetric, we just need to consider the spacial projections onto the $r - \theta$ plane. The boundary of the flow is a spherical shell at $r = r_0$ from which test particles are continuously injected. On the shell, the four velocities of particles are taken to be constants, i.e.,

$$u^r(r_0, \theta) = u^\theta(r_0, \theta) = u^\phi(r_0, \theta) = \text{const.}, \quad (122)$$

with which and identity $g_{\mu\nu}u^\mu u^\nu = -1$, u^t can be obtained. u^μ at r_0 are taken as the initial conditions for the calculation of geodesics. Using Equation (77) the physical velocities v_r, v_θ, v_ϕ can be computed from u^μ . Then the constants of motion are uniquely determined. The results are illustrated in Figure 9, which agree well with those of Tejeda et al. (2013).

6.6. The tidal disruption of a ball

As the final application of our code we use it to mimic a tidal disruption event of a ball, which falls freely to the central black hole. To use the code, we have to assume that the ball is consists of a set of equal mass test particles without any interactions. At the initial point the ball has a kick velocity, the physical components of which measured under the LNRF reference are v_r, v_θ, v_ϕ . And all of the particles share the same initial velocities but different positions. Then with the given initial conditions, each particle falls inward freely along a geodesic trajectory.

In Figure 10, we show the deformed images of the ball for five different coordinate times. At initial moment, we assume that the shape of ball is a regular sphere and the center of the ball is located in the equatorial plane of the black hole. The velocities are $v_r = -0.1, v_\theta = 0, v_\phi = 0.1$. One can see that the shape of the ball is significantly deformed and stretched as it approaches

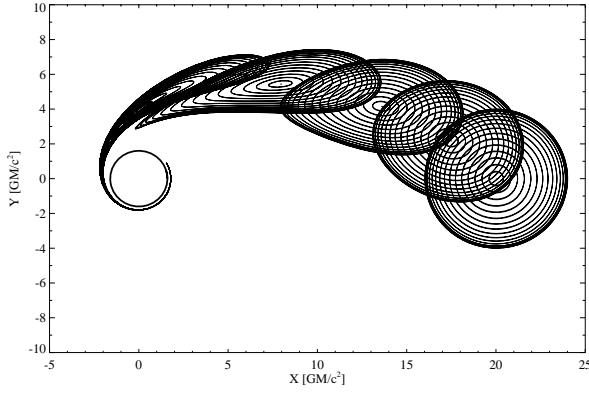


Fig. 10. An assumed ball composed by a set of massive test particles without interactions is disrupted by the strong tidal force of a Kerr black hole. The black hole spin $a = 0.8$. The radius of the ball is $4 r_g$. The initial coordinates are $r = 20 r_g$, $\theta = 90^\circ$, $\phi = 0^\circ$. The coordinate times are $t = 0, 22.5, 45, 67.5, 90$ for images from right to left. A circle in the left represents the event horizon.

to the central black hole due to the strong tidal disruption force. And the former part is stretched more seriously than the latter part. The debris of ball orbits around the black hole along a spiral trajectory and goes inward slowly instead of falling into the black hole directly for the frame drag effect. However, the picture illustrated by this example is a toy model definitely.

7. Discussion and conclusion

We have developed a new fast public code named ynogkm for calculating time-like geodesics under a K-N spacetime, which is a direct extension of Yang & Wang (2013). In ynogkm, we adopt the same strategies used in ynogk, i.e., expressing all coordinates and proper times as functions of a parameter p and calculating all elliptic integrals by Carlson's approach. The former guarantees the convenience of the code in practice application and the latter guarantees the fast speed of the code respectively. The extension is involved in many more complicated cases.

In the expressions, we also use the Weierstrass' elliptic function $\wp(z; g_2, g_3)$ and integral as investigated by many authors in the literature. By this way they not only investigate the geodesic motion itself but also the properties of the spacetime. While what we discussed in this paper focus on the potential real applications of the calculation of geodesic orbits in astrophysics. In order to avoid the complex integrals, we also adopt the Jacobi's elliptic functions $\text{sn}(z|k^2)$, $\text{cn}(z|k^2)$ when equation $R(r) = 0$ has no real roots.

Since ynogkm uses the same strategies with ynogk, their speed are almost the same, we do not present the speed test results. As discussed in Chan et al. (2013), a powerful approach improving the speed of tracing the trajectories of billions of photons in a curved spacetime is based on the massively parallel algorithm and GPU graphic cards. Their results show that this approach is two orders of magnitude faster than the CPU-based tracing codes. Therefore the extension of ynogkm from a serial program to a parallel program is the future work.

To demonstrate the utility of ynogkm, we just apply it to six toy problems and present the results simply. Its application to more complicated and practical cases will be given in the future works.

Acknowledgments

We acknowledge the anonymous referee for his/her valuable comments and advices, which significantly improve the manuscript. We acknowledge the financial supports from the National Natural Science Foundation of China 11133006, 11163006, 11173054, the National Basic Research Program of China (973 Program 2009CB824800), and the Policy Research Program of Chinese Academy of Sciences (KJXC2-YW-T24).

References

- Abramowitz, M., & Stegun, I. A. 1965, Handbook of mathematical functions with formulas, graphs, and mathematical tables (Dover Books on Advanced Mathematics, New York: Dover)
- Bardeen, J. M., Press, W. H., & Teukolsky, S. A. 1972, ApJ, 178, 347
- Carlson, B. C. 1988, Mathematics of Computation, 51, 267
- Carlson, B. C. 1989, Math. Comp., 53, 327
- Carlson, B. C. 1991, Math. Comp., 56, 267
- Carlson, B. C. 1992, Mathematics of Computation, 59, 165
- Carter, B. 1968, Physical Review, 174, 1559
- Chan, C.-K., Psaltis, D., & Ozel, F. 2013, arXiv:astro-ph/1303.5057
- Cunningham, C. T., & Bardeen, J. M. 1973, ApJ, 183, 237
- Cunningham, C. T. 1975, ApJ, 202, 788
- Dexter, J., & Agol, E. 2009, ApJ, 696, 1616
- Hackmann, E. 2010, PhD thesis, University of Bremen
- Hackmann, E. Xu, H. X. 2013, arXiv:/1304.2142H
- Li, L.-X., Zimmerman, E. R., Narayan, R., & McClintock, J. E. 2005, ApJS, 157, 335
- Luminet, J. P. 1973, A&A, 75, 228L
- Mino, Y. 2003, PhRvD, 67, 084027
- Misner, C. W., Thorne, K. S., & Wheeler, J. A. 1973, Gravitation (San Francisco: W.H. Freeman and Co.)
- Press, W. H., Teukolsky, S. A., Vetterling, W. T., & Flannery, B. P. 2007, Numerical recipes in FORTRAN. The art of scientific computing (Cambridge: University Press, —c2007, 3rd ed.)
- Rauch, K. P., & Blandford, R. D. 1994, ApJ, 421, 46
- Shakura, N. I. 1987, Sov. Astron. Lett., 13, 99
- Tejeda, E., Taylor P. A., Miller J. C. 2013, MNRAS, 429, 925
- Wang, Y., & Li, X.-D. 2012, ApJ, 744, 186
- Wilkins, D. C. 1972, PhRvD, 5, 814
- Yang, X.-L., & Wang, J.-C. 2013, ApJS, 207, 6

Appendix A: The transformation matrix

Here we discuss how to get the explicit expression for the matrix T , which transform the physical velocities v'_x, v'_y, v'_z of a particle specified in the reference of the tetrad $\mathbf{e}'_x, \mathbf{e}'_y, \mathbf{e}'_z$ into the LNRF reference whose origin is fixed at the same point. As shown in Figure A.1, we have four references, i.e., R' : $\{p, \mathbf{e}'_x, \mathbf{e}'_y, \mathbf{e}'_z\}$, R'' : $\{O, x'', y'', z''\}$, R : $\{O, x, y, z\}$, and $R_{r\theta\phi}$: $\{p, \mathbf{e}_r, \mathbf{e}_\theta, \mathbf{e}_\phi\}$.

The matrix of transformation T_1 from R' into R'' can be gotten directly,

$$\begin{pmatrix} v''_x \\ v''_y \\ v''_z \end{pmatrix} = \begin{pmatrix} -\sin \varphi & -\cos \varphi & 0 \\ \cos \varphi & -\sin \varphi & 0 \\ 0 & 0 & 1 \end{pmatrix} \begin{pmatrix} v'_x \\ v'_y \\ v'_z \end{pmatrix}. \quad (\text{A.1})$$

The transformation T_2 from R'' into R is given by,

$$\begin{pmatrix} v_x \\ v_y \\ v_z \end{pmatrix} = \begin{pmatrix} \cos \gamma \cos \beta & -\sin \gamma & \cos \gamma \sin \beta \\ \sin \gamma \cos \beta & \cos \gamma & \sin \gamma \sin \beta \\ -\sin \beta & 0 & \cos \beta \end{pmatrix} \begin{pmatrix} v''_x \\ v''_y \\ v''_z \end{pmatrix}. \quad (\text{A.2})$$

The transformation T_3 from R into $R_{r\theta\phi}$ is given by,

$$\begin{pmatrix} v_r \\ v_\theta \\ v_\phi \end{pmatrix} = \begin{pmatrix} \cos \psi \sin \theta & \sin \psi \sin \theta & \cos \theta \\ \cos \psi \cos \theta & \sin \psi \cos \theta & -\sin \theta \\ -\sin \psi & \cos \psi & 0 \end{pmatrix} \begin{pmatrix} v_x \\ v_y \\ v_z \end{pmatrix}. \quad (\text{A.3})$$

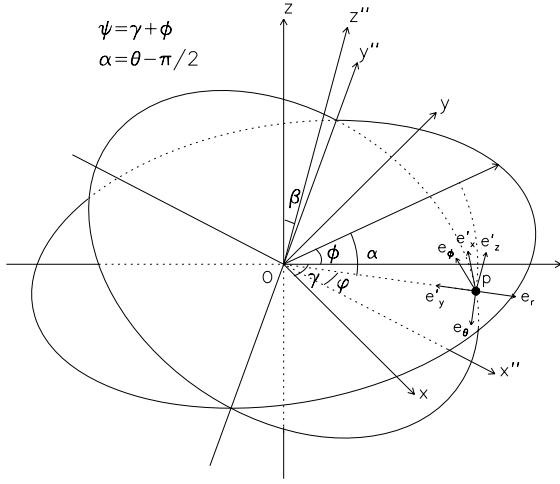


Fig. A.1. The geometry between the skewed disk plane and the equatorial plane of a black hole. The boundary of the disk is a ring, at which equal mass test particles are injected continuously. At the initial position, indicated by p , there are two orthonormal tetrads, i.e., $\{p, \mathbf{e}_r, \mathbf{e}_\theta, \mathbf{e}_\phi\}$ and $\{p, \mathbf{e}'_x, \mathbf{e}'_y, \mathbf{e}'_z\}$. In order to compute the constants of motion, we need to transform the initial physical velocities of a particle v'_x, v'_y, v'_z , which are specified by $\{p, \mathbf{e}'_x, \mathbf{e}'_y, \mathbf{e}'_z\}$, into $\{p, \mathbf{e}_r, \mathbf{e}_\theta, \mathbf{e}_\phi\}$.

Thus the transformation T from R' into $R_{r\theta\phi}$ is given by

$$T = T_3 T_2 T_1, \quad (\text{A.4})$$

and noting that $\psi = \gamma + \phi$, one has

$$T_3 T_2 = \begin{pmatrix} \sin \theta \cos \phi \cos \beta - \cos \theta \sin \beta & \sin \theta \sin \phi & \\ \cos \theta \cos \phi \cos \beta + \sin \theta \sin \beta & \cos \theta \sin \phi & \\ -\sin \phi \cos \beta & \cos \phi & \\ \sin \theta \cos \phi \sin \beta + \cos \theta \cos \beta & & \\ \cos \theta \cos \phi \sin \beta - \sin \theta \cos \beta & & \\ -\sin \phi \sin \beta & & \end{pmatrix}.$$

Finally one gets

$$T = \begin{pmatrix} 0 & -1 & 0 \\ -\sin \phi \sin \beta & 0 & -\sqrt{1 - \sin^2 \phi \sin^2 \beta} \\ \sqrt{1 - \sin^2 \phi \sin^2 \beta} & 0 & -\sin \phi \sin \beta \end{pmatrix}. \quad (\text{A.5})$$

In the reduction, the following identities are used

$$\sin \theta = \frac{\cos \beta}{\sqrt{1 - \sin^2 \phi \sin^2 \beta}}, \quad (\text{A.6})$$

$$\cos \theta = -\frac{\cos \phi \sin \beta}{\sqrt{1 - \sin^2 \phi \sin^2 \beta}}, \quad (\text{A.7})$$

$$\sin \varphi = \frac{\sin \phi \cos \beta}{\sqrt{1 - \sin^2 \phi \sin^2 \beta}}, \quad (\text{A.8})$$

$$\cos \varphi = \frac{\cos \phi}{\sqrt{1 - \sin^2 \phi \sin^2 \beta}}. \quad (\text{A.9})$$

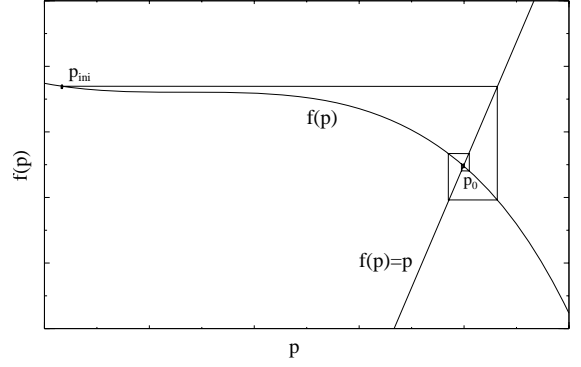


Fig. B.1. The curve of $f_\sigma(p)$ (or $f_t(p)$) as function of p . p_0 is the unique real root of equation $\sigma(p) = \sigma_0$ (or $t(p) = t_0$). Starting from an appropriate initial value, p_{ini} , one can approach to p_0 through an iterative process.

Appendix B: Taking t and σ to be the independent variable

In some practical applications, one prefers using t or σ as the independent variable than parameter p . Since we have expressed all B-L coordinates and proper times as functions of the parameter p , when a value of t or σ is given, there is a unique p corresponds to it. Namely, both the equations $t(p) = t_0$ and $\sigma(p) = \sigma_0$ have one and only one real root, which is denoted by p_0 . Apparently, if we can solve these equations efficiently and precisely to get p_0 , we can take t or σ as the independent variable, for p_0 is obtained, the other three coordinate r, μ , and ϕ are also uniquely determined.

Actually we can solve both the equations $t(p) = t_0$ and $\sigma(p) = \sigma_0$ by bisection method or iterative method. From the expressions for t_r, t_μ and σ_r, σ_μ given in Section 3.3.2 we can rewrite functions $t(p)$ and $\sigma(p)$ as

$$\sigma(p) = \bar{\sigma}(p) + C_\sigma p, \quad (\text{B.1})$$

$$t(p) = \bar{t}(p) + C_t p, \quad (\text{B.2})$$

where the definitions of C_σ and C_t are given in table 7. Thus for a given σ_0 and t_0 , we have

$$p = \frac{\sigma_0 - \bar{\sigma}(p)}{C_\sigma} = f_\sigma(p), \quad (\text{B.3})$$

$$p = \frac{t_0 - \bar{t}(p)}{C_t} = f_t(p). \quad (\text{B.4})$$

We illustrate schematically how to solve these equations by iterative method in Figure B.1. To use the bisection method, we define two new functions

$$F_\sigma(p) = f_\sigma(p) - p, \quad (\text{B.5})$$

$$F_t(p) = f_t(p) - p. \quad (\text{B.6})$$

From Figure B.1, we can see that when $p < p_0$, $F_\sigma(p)$ or $F_t(p) > 0$; when $p > p_0$, $F_\sigma(p)$ or $F_t(p) < 0$. Thus through the use of bisection method, we can solve the equations $F_\sigma(p) = 0$ and $F_t(p) = 0$ immediately.

Table 7.

Case	C_σ, C_t
1	$C_\sigma = a^2 \mu_{\text{tp}_1}^2 + r_{\text{tp}_1}^2,$ $C_t = C_\sigma + (2 + e\varepsilon)(2 + r_{\text{tp}_1}) - e^2 + A_{t+} - A_{t-},$
2, 3	$C_\sigma = a^2 \mu_{\text{tp}_1}^2, \quad C_t = C_\sigma + \frac{1}{\sqrt{ 1 - m^2 }} [2(2 + e\varepsilon) - e^2],$
4, 5	$C_\sigma = b_1^2 + \frac{a^2 \mu_0^2}{2}, \quad C_t = C_\sigma + (2 + e\varepsilon)(2 - b_1/b_0) - e^2.$

¹ $\mu_0 = \sqrt{q/(q + \lambda^2)}$.